FABRICATION AND IN VITRO CHARACTERIZATION OF AN IMPLANT FOR THE DETECTION OF METASTATIC CANCER CELLS

By

CARLOS MARTÍN CANTÚ

Presented to the Faculty of the Graduate School of

The University of Texas at Arlington in Partial Fulfillment

of the Requirements

for the Degree of

MASTER OF SCIENCE IN BIOMEDICAL ENGINEERING

THE UNIVERSITY OF TEXAS AT ARLINGTON

Spring 2018

Acknowledgements

My sincerest acknowledgements go to Ashley Dacy, for her technical and theoretical expertise, which greatly aided my ability to manufacture, design, and test the implants. I would like to thank Christian Griffith for providing the phantom tissue and helping me with the subcutaneous insertion of the implants into the deceased mouse. I also would like to offer my appreciation towards Amirhossein Hakamivala, who gave me technical and pragmatic direction during my project and the two years I worked as a research assistant. I also extend my deepest regards, respect, and gratitude towards Dr. Liping Tang, for his scientific advice and support throughout the project as well as the opportunity to work and learn in his laboratory. I also must stress the friendship that I hold with these great individuals, especially Mr. Hakamivala, it certainly helped me maintain my focus and good spirits throughout my time as a graduate student, in addition to motivating my goal to become a great scientist.

Abstract

FABRICATION AND IN VITRO CHARACTERIZATION OF AN IMPLANT FOR THE DETECTION OF METASTATIC CANCER CELLS

Carlos Martín Cantú, MS

The University of Texas at Arlington, 2018

Supervising Professor: Liping Tang

Greater than 90% of cancer related deaths are due to metastasis (Hayes & Wicha, 2011). Since current conventional techniques detect the disease by the time that it has become systemic, our lab has developed a hydrogel based cancer trap that can attract metastatic cancer cells via cytokine release. However, for continual monitoring and accessibility to the gel, an implant is needed for delivery, retention, and retrieval of the gel. The research undergone in this thesis seeks to develop such a method. Namely, the objective was to develop a polylactide (PLA) based implant that is capable of delivering and retaining a polyethylene glycol based gel, which is filled with cytokines for attracting metastatic cancer cells, in subcutaneous space for continual monitoring of the potential progression of localized cancer cells to a metastatic state.

Table of Contents

LIST OF TABLES

Table of Figures

Chapter 1

Chapter 2

Chapter 3

Chapter 4

Chapter 1

Introduction

1.1 Cancer Trap Device

Due to the high rate of mortality resulting from cancer metastasis, it would be ideal to detect cancer cells before or when they assume a metastatic state. Conventional diagnostic methods, such as magnetic resonance imaging (MRI), computed tomography (CT), positron emission tomography (PET), ultrasound, and traditional radiography (X-ray), detect cancer by the time that it has become systemic (Fass, 2008). In addition, current therapeutic methods, such as chemotherapy and immunotherapy, do not target circulating cancer cells precisely for elimination. Recent trends involve the development of methods that target circulating tumor cells (CTCs), such as the FDA approved CellSearch System® (Hong & Zu, 2013). These detection systems use a similar general approach (Figure 1.1) that involves collection of blood from a patient and tumor cell isolation, subsequent tumor cell staining or oncogene probing, and finally the detection of CTCs via different molecular and cellular techniques (Hong & Zu, 2013). These emerging methods do hold certain technical obstacles, such as inconsistent results in CTC detection rate and correlation between CTC presence and survival rate (Paterlini-Brechot et al., 2007; Nagaiah & Abraham, 2010; Alunni-Fabbroni & Sandri, 2010). In addition, these methods detect circulating tumor cells from blood samples, which likely accounts for the inconsistent results and also would mean that cancer cells may already be infiltrating other distant areas since they are already in the circulation.

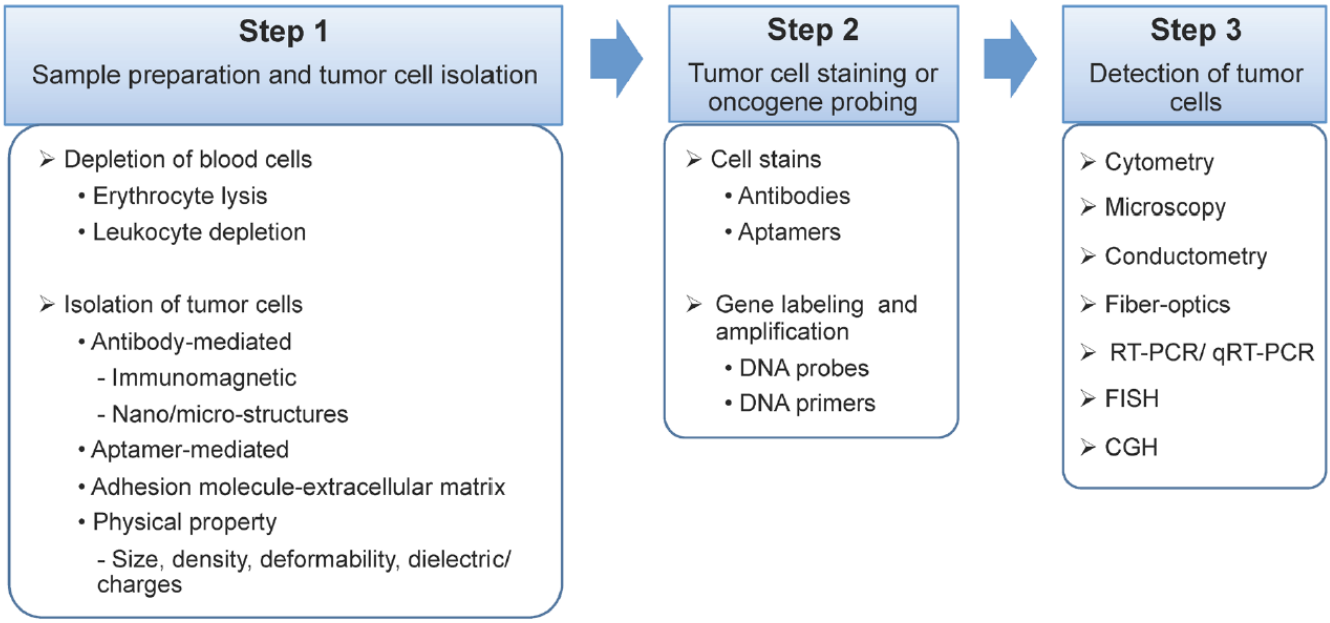

Figure 1.1 Schematic for three major steps of CTC assay. Step 1. Sample and tumor cell isolation: Reduction or filtration of blood cells, selective isolation of tumor cells from blood cells via different methods. Step 2. Tumor cell staining or oncogene probing with antibodies/aptamers and DNA probes/primers. Step 3. Detection of tumor cells via different cell and molecular techniques.

Thus, there is need for a more effective device that can detect metastasis at earlier stages that have been defined biologically, such as in carcinomas, which have been found to initially spread to lymph nodes near the initial tumor before draining into the venous system and hence other parts of the body (Kumar, Abbas, Fausto, Robbins, & Cotran, 2005). Also, there is need to selectively increase the amount of tumor cells found in the acquired sample to be assessed, to reduce inconsistent quantifications seen with current CTC devices. Motivated by the concept of the Roach Motel®, which attracts and captures roaches by pheromone release, our lab has fabricated a scaffold that is capable of recruiting cancer cells by cytokine release in a murine melanoma metastasis model (Ko et al., 2012). Namely, our lab showed that scaffolds loaded

with erythropoietin but not stromal cell-derived factor-1α were significantly more efficient at recruiting labeled B16F10 melanoma cells (Figure 1.2A, B) and increasing survival (Figure 1.2C).

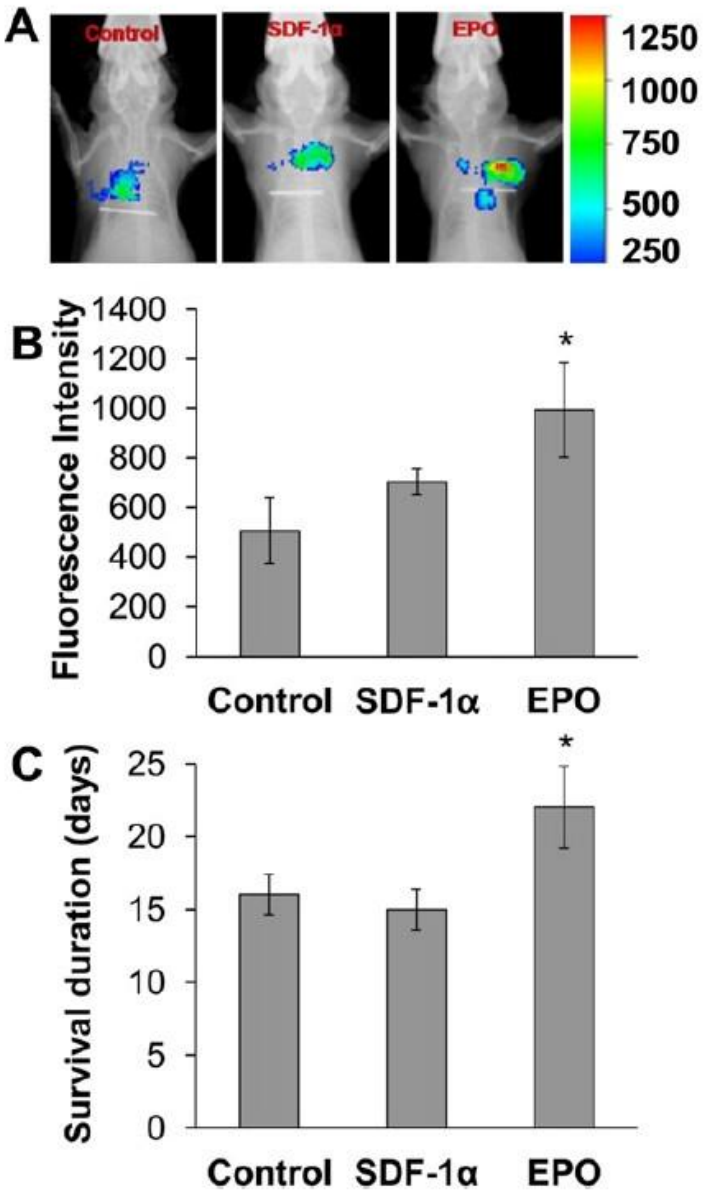

Figure 1.2 Real time in vivo imaging assessing recruitment of labeled B1610 melanoma cells to poly (lactic-co-glycolic acid) scaffolds loaded with erythropoietin (EPO), stromal cell-derived factor-1α (SDF-1α), and non-loaded control. (A) Real time *in vivo* imaging showing accumulation of B16F10 melanoma cells around scaffolds. The fluorescence intensity comparison (B) shows enhanced accumulation of melanoma cells and the survival duration (C) is also significantly higher in EPO releasing scaffolds. $p<0.05$

Melanoma and inflammatory cell recruitment in relation to different biomaterials was also characterized (Figure 1.3A, B). The results articulate the higher recruitment of inflammatory and melanoma cells on PLA based biomaterials versus aluminum and glassperien. In addition, there was high correlation (R^2=0.9197) between the recruitment of inflammatory and melanoma cells (Figure 1.3C).

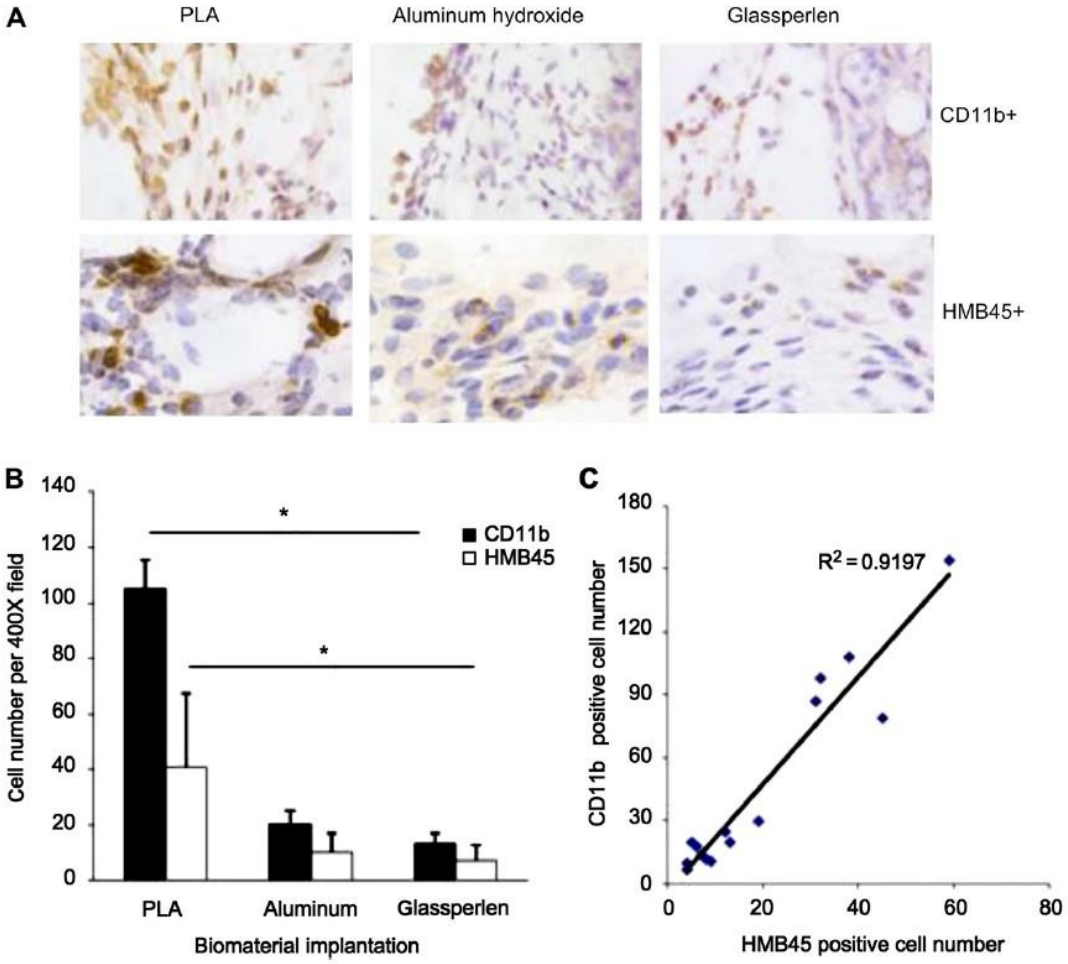

Figure 1.3 Extent of inflammatory and melanoma cell recruitment. Immunohistochemistry (A) for CD11b+, inflammatory cell marker, and HMB45+, melanoma cell marker, was done on PLA, aluminum hydroxide, and glassperien, where positive cells are stained yellowish-brown. Their recruitment of CD11b+ and HMB45 stained cells was quantified and compared (B). The correlation (C) between stained CD11b+ and HMB45 was statistically analyzed. $p<0.05$*

Further support for the role of the inflammatory response in mediating melanoma cell reduction is exemplified by the significant reduction of both inflammatory and melanoma cells with an anti-inflammatory drug, as exemplified in Figure 1.4.

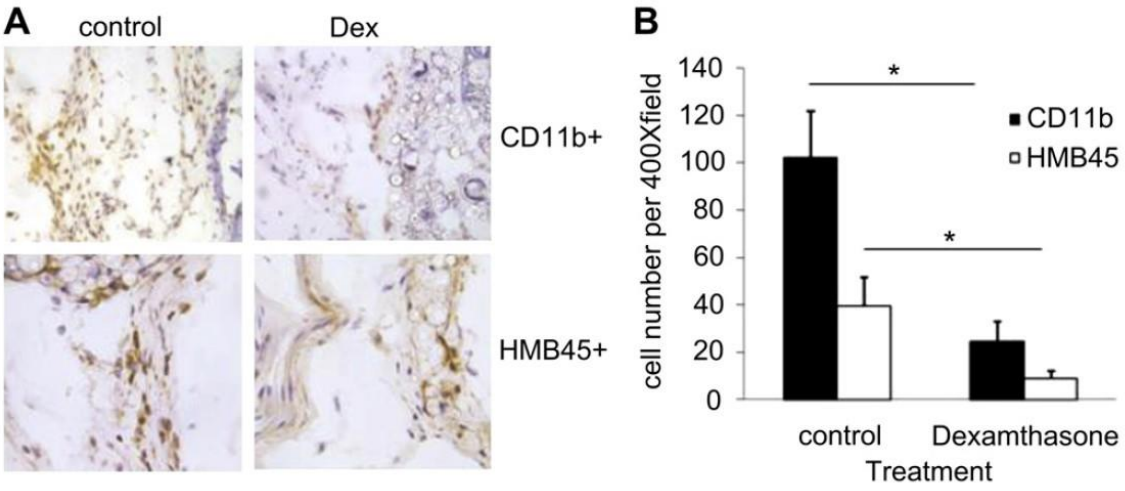

Figure 1.4 Comparison of inflammatory (CD11b+) and melanoma (HMB45+) recruitment under dexamethasone treatment. The immunohistochemical staining (A) shows recruitment of inflammatory cells for PLA microspheres (top left), dexamethasone soaked PLA microspheres (top right) and melanoma cells for polylactide microspheres (bottom left) and dexamethasone soaked PLA microspheres (bottom right), where positive cells are stained yellowish-brown. Quantification of the cell numbers (B) were statistically analyzed. $p<0.05$ *

Overall, the past studies done in our labs exemplify the application of polyanhydride based devices for recruiting and capturing cells via inflammatory mechanisms rendered by the foreign body response or via cytokine release. These experiments have led to the idea of cancer trapping, that is, selective capture of migrating cancer cells via chemotaxis. The cancer trap was patented as a biodegradable hydrogel scaffold intended for therapeutic or diagnostic purposes (U.S. Patent No. 20150283073). Subsequent studies that replicate the use of polyanhydride based implants and the ensuing inflammatory response for cancer cell recruitment have found similar

results. Rao et al. (2016) showed that by implantation of cylindrical, porous polycaprolactone implants, cancer cell recruitment can be achieved by the resultant inflammatory response and lead to tumor reduction as illustrated in Figure 1.5.

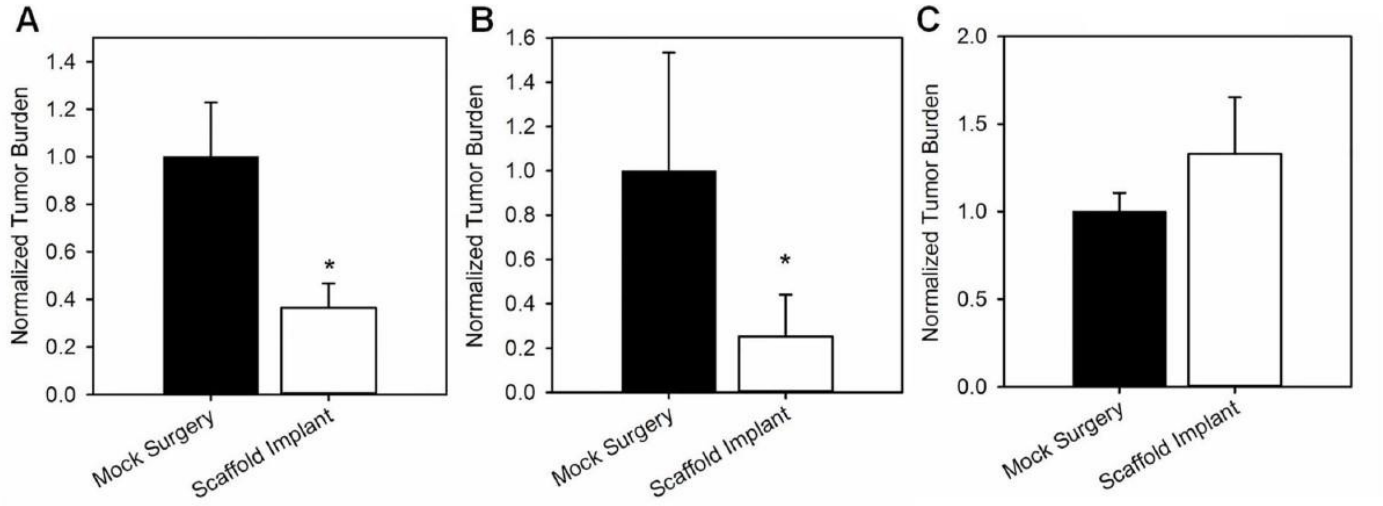

Figure 1.5 Statistical Analysis representation of reduced tumor burden in (A) liver, (B) brain, and (C) lung. The scaffold implants were not loaded with any bioactive substance such as cytokines or growth factors. $p<0.5$ *

A previous study from the same group reported a similar outcome (Figure 1.6) with poly (lactide-co-glycolide) (PLGA) based implants (Azarin et al., 2015). Overall, these studies support our original findings and concept of a trap that can target cancer cells by chemotaxis recruitment rather than honing in on them. The incorporation of polyanhydrides as a material for implants and medical devices has much potential in therapeutic and diagnostic applications in cancer.

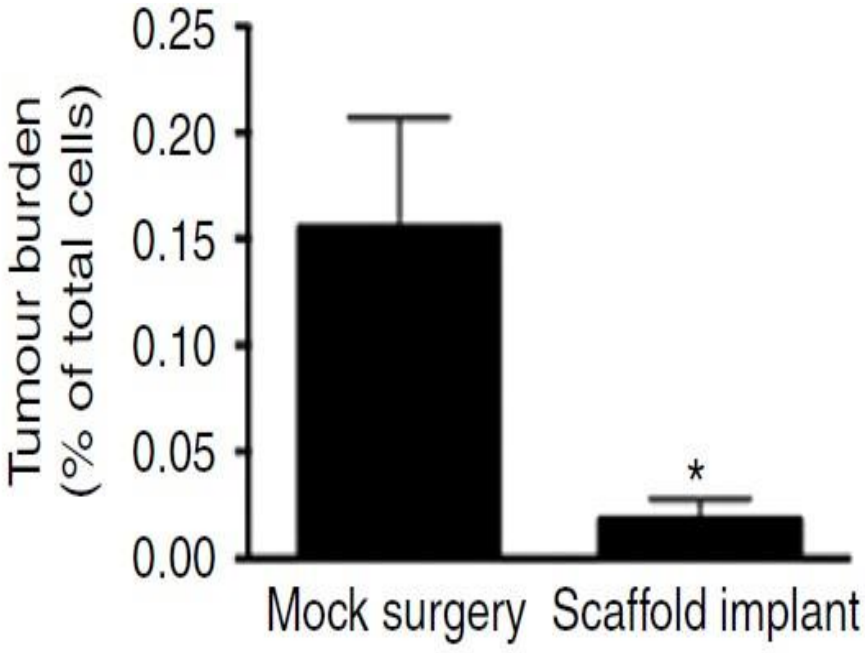

Figure 1.6 Comparison of tumor cell numbers isolated from the lung at day 28 post-tumor inoculation. The scaffold implant was a polycaprolactone implant with no drugs or growth factors loaded on it.
$p<0.05$*

Despite the promising results that the cancer trap has shown in recruiting metastatic cancer cells and enhancing survivability, there is still need for characterizing a retrieval method for the hydrogel. This would allow the cancer trap to be used for diagnostic purposes, namely through the injection of fresh hydrogel, subsequent removal of hydrogel infiltrated with tumor cells and respective analysis, and injection of fresh media again into the same area of the body. This cycle would be repeated over a determined period of time to monitor possible metastasis and state of a given tumor. Accordingly, the aim of this thesis was to develop a 3-D printed implant that can deliver the hydrogel into the body, allow feasible gel retrieval from it while inside the body, and allow optimal cytokine release and infiltration of cancer cells into it.

1.2 Computer Assisted Design (CAD) and 3-D Printing

Highly used methods in tissue engineering for the creation of scaffolds include fiber bonding, phase separation, solvent casting, particulate leaching, membrane lamination, molding and foaming (Yang et al., 2001). They are great methods for scaffold fabrication, but they do not offer much control over the pore size homogeneity and pore structure. CAD and 3-D printing, also known as rapid prototyping and additive manufacturing, offer more control over the pore size and structure that can be defined in a scaffold or implant (Yang et al., 2002; Yeong et al., 2004). The overall geometry, porosity, and pore size can be adjusted in different ways to affect the mechanical strength and stiffness. Accordingly, matching stiffness, porous gradient, and mechanical strength between a porous scaffold and target tissue structure's properties becomes more feasible (Leong et al., 2008). Based on these advantages, CAD and 3-D printing was used to fabricate the implant for the cancer trap.

Different forms of 3-D printing processes can be applied to tissue engineering purposes. Namely, they can be separated based on printing materials and manufacturing process as seen in Table 1.1 (Jasiuk et al., 2018). Overall, all of these methods do share certain features: (1) The design is created in 3-D or 2-D with CAD software. (2) The design is converted to STL file format and then digitally updated by 3-D printing programs into distinct printable layers read by the printer. (3) The raw materials are processed into filaments, binder solutions, and granules for the printing process. (4) The materials are added and solidified layer by layer, ultimately rendering a target product. (5) Some products require post-processing steps, such as sintering, polishing, or smoothing the surface (Norman et al., 2017).

Table 1.1 Overview of different materials and processes for Rapid Prototyping

Process	Description	Advantages	Disadvantages
Powder bed fusion (PBF)	1. A roller or blade is used to deposit a thin layer of powder on a build plate 2. Laser fuses certain areas in the powder 3. Build plate is lowered by the height of the powder layer 4. Repeat steps 1–3 for height of part 5. Excess powder is removed	- Excess powder serves as support, so no support structures required[6] - Superior mechanical properties[7,8]	- Expensive, high material waste[9] - Few compatible materials[10] - Rough or grainy surface
Typical materials	*Polystyrene, polyester, polyamide 11 and 12, polypropylene, polyurethane, polyetheretherketone (PEEK)*		
Material jetting	1. Liquid polymer is jetted onto a build plate in droplets 2. Ultraviolet (UV) source cures the polymer 3. Build plate is lowered or print head is raised by the height of the droplet layer 4. Repeat steps 1–3 for height of part 5. Support material is removed	- Manufacture multimaterial parts[11] - Low residual stresses[12] - High dimensional accuracy[13,14]	- Weak mechanical properties[15] - Adverse environmental effects[16]
Typical materials	*Acrylates, acrylics, polylactic (PLA), epoxies, starch*		
Vat photopolymerization	1. Build plate is positioned on top of a vat of photopolymer 2. UV source below vat cures certain areas in thin layer contacting the build plate 3. Build plate is raised by thickness of cured layer 4. Repeat steps 1–3 for height of part 5. Support material is removed	- High resolution to build time ratio[17] - Good durability[18] - Can produce multimaterial parts, but it is difficult[19]	- Relatively expensive due to requirement for vat change[20,21] - Requires support material - Cannot create parts with enclosed volumes due to liquid environment[22]
Typical materials	*Acrylates, acrylics, epoxies*		
Material extrusion	1. Thermoplastic filament is passed through a heated print head as the print head moves over certain areas of a build plate 2. Once the layer is complete, either the print head or build plate moves by height of layer 3. Repeat steps 1 and 2 for height of part 4. Support material is removed	- Can be optimized for strong material properties[23–25] - Low costs of machines[26,27]	- Low resolution and poor surface finish require significant postprocessing[28,29] - High residual stresses[30]
Typical materials	*Acrylonitrile butadiene styrene (ABS), PLA, acrylics, polycarbonate (PC), polyetherimide (PEI), high impact polystyrene*		

Fused deposition modeling (FDM) is one of the most widely used 3-D printing processes. The main materials used in FDM are polymeric filaments and due to the inexpensive equipment as well as non-volatile, non-aerolizing materials used, FDM is popular for many manufacturing

settings or purposes, including home use (Azimi et al., 2016; Steinle, 2016; Kim et al., 2015). In addition, some of the polymeric filaments that can be printed from FDM are FDA approved polymers, such as PLA and PCL. This latter characteristic motivates the use of these materials in FDM for medical purposes, such as implants, prosthetics, scaffolds, and hearing aids (Jasiuk et al., 2018). PLA is highly utilized for medical applications because of its biodegradability and low level of shrinkage, which results in less deformation and delamination that leads to less internal stresses and better mechanical characteristics (Tymrak et al., 2014; Kuznetsov et al., 2018). Thus, PLA was selected for manufacturing the implants.

Chapter 2

Design and 3-D Printing

2.1 Rationale

The overall design was intended to allow feasible gel accessibility and cancer cell recruitment. The implant also was aimed to be mechanically stable to ensure that the gel is not lost during its placement inside subcutaneous space. In addition, it should allow feasible injection and retrieval of gel from subcutaneous tissue, contain a cylinder-shaped profile, and have a total pore area/total surface area ratio as high as possible. In addition, the design was made with a 10-15 mm length, minimal inner diameter of 3.5 mm, and a thickness of 0.5 mm. The cylinder shaped outline is selected because the delivery device uses a cylinder shaped cannula to deliver the implant. A high total pore area/total surface area ratio was desired to render high cytokine release and cell infiltration from and into the gel. The length range chosen was to minimize invasiveness of the procedure for implantation, based on previously manufactured subcutaneous implants (Kleiner et al., 2014). The original design and manufacture method included making pores with a diameter ranging from 0.6 mm to 1mm and making the implants smooth through post-processing techniques. The reason for making the implant smooth is based on past research that exemplifies the preferment of cancer cells to attach to rough rather than smooth surfaces (Chen et al., 2013). Difficulties in reproducibility and limitations with FDM led to consideration of making designs with pores that are larger than 1 mm. Other modifications were also implemented on the design to improve the reproducibility and function of the capsular, porous implants. In addition, designs that resembled a cage-like

appearance were also developed and some were printed successfully. They were intended to provide more accessibility than the capsular, porous design, however it was also possible that they lose mechanical strength. The best designs in terms of attained total pore area/total surface area ratio would then be further evaluated on their mechanical properties and ability to retain gel and allow retrieval from it while in subcutaneous space.

2.2 Methods

2.2.1 CAD design

All designs were made in SolidWorks® 2017. Two main types of designs were implemented. One design was capsular, porous while the other had a cage-like appearance. The capsular, porous designs then were further defined based on pore shape, which was circular or slotted, and pore diameter size, which was 0.6 mm to 1mm or larger than 1 mm. Cage-like were further specified into either a grated or long gap design. These denominations are summarized in Figure 2.1. All capsular designs, in addition to the grated cage-like, had an inter-pore spacing of approximately 1/3 to 1/2 of the diameter length, which was found to be optimal for minimizing merging of the pores or the pores getting filled in with filament. All designs had an approximate inner diameter of 3.5 mm and outer diameter of 4 mm. The files were saved as STL files for importation into Slic3r® software to specify the pattern of extrusion and printing parameters.

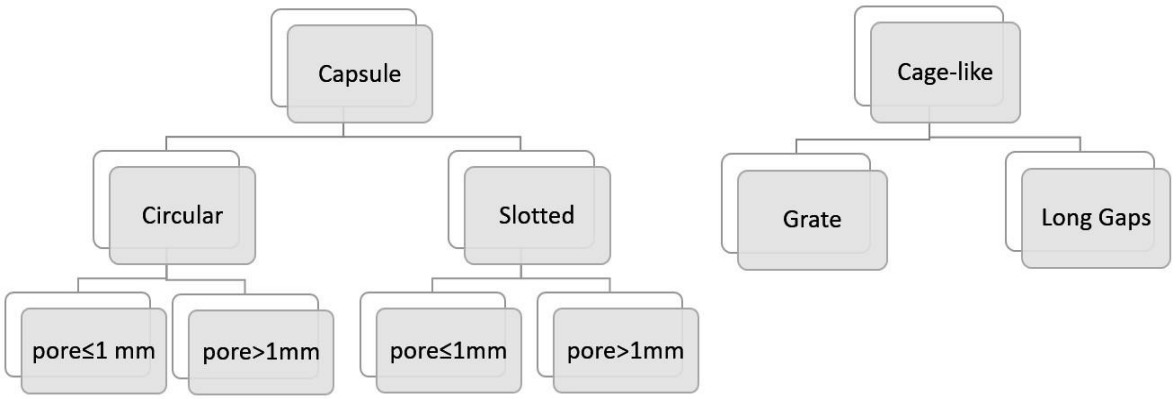

Figure 2.1 Design specification for capsule and cage-like implants. Pore refers to pore diameter (mm) in the circular designs and length (mm) in the slotted designs.

2.2.2 Materials and 3-D printing

a. materials

The types of filament used were white and black 1.75 mm PLA. They were purchased from Hatchbox®. Both the white and black filaments were characterized by a print temperature ranging from 180°C-220°C and a dimensional accuracy of ±0.03 mm. The filaments are a blend of plant-based materials and polymers, which are not specified by the manufacturer.

b. 3-D printing

The 3-D printing method used was FDM and the type of printer was a GMax 1.5x. In addition, the extruder was preheated to 200°C before initiating the printing with black filament. The speed of the extrusion was set at 10% when forming the first layer of all designs. The speed was then increased to 30-50%, depending on the printing progression. The implants were printed along the z-axis.

2.2.3 Slic3r® parameters

Slic3r®, a software used for importing STL files and exporting them in g code to a rapid prototyping device, was used to specify the printing parameters. The fan speed was initially set at a minimum of 40% and a maximum of 60%, it was later set at a minimum of 55% and maximum of 75%. Temperature was set at either 190 °C or 200°C for both filaments. Layer height was initially set to 0.2 mm and later at 0.1 mm.

2.2.4 Calculation of total pore area/total surface area ratio

Pictures of 3-D printed implants were taken with a smartphone and then imported into Image J. A scale was placed next to the implants to serve as a reference for distance. Image J was then utilized for calculations, namely the most representative open pores and gaps were assessed in terms of area and then a pore area and gap area average was obtained for the assessed pores and gaps. This average value was then multiplied with the amount of open pores and gaps to find the total open area for pores and gaps. This total open area was then added to the area of the injection port. This resultant area was then divided by the total surface area. The total pore area/total surface area ratio fidelity was calculated by dividing the actual ratio by the corresponding theoretical ratio.

2.2.5 Pore and Gap Area Fidelity

The pore fidelity was calculated for implants. It was calculated by dividing the average actual pore and gap areas by the respective theoretical areas defined on the initial CAD designs.

2.2.6 Post-processing

For attaining a smooth surface, implants received smoothing with ethyl acetate, dichloromethane (DCM), and chloroform. The two forms of smoothing attempted were vaporization and dipping in either of these three solvents.

a. vaporization

A 50 ml Erlenmeyer flask was filled with 7-10 ml of either of the three solvents. This flask was then sealed loosely with a rubber stopper. The flask was then placed on a hot plate and the temperature was set to the boiling temperature of the given solvent. After about 5-8 minutes, depending on the solvent, the flask will be filled with vapor. The rubber stopper is then removed and, with the use of tweezers, the PLA sample or implant is held within the Erlenmeyer flask opening for 2-5 s without it making contact with the liquid solvent and condensation on flask walls. If more smoothing is desired, the flask is filled with vapor again and the implant is held within the flask for another 2-5 s. The latter step is repeated as much times as necessary to obtain the desired finish.

b. dipping

A 50 ml beaker was filled with enough solvent to immerse sample or implant, usually about 10-12 ml. The sample or implant is immersed for 2-6 s inside the solvent and then placed outside to dry. If more smoothing is required, the part or implant would be dipped again and then placed outside to dry.

2.3 Results

2.3.1 Post-processing tests with PLA samples

Figure 2.2 shows two examples of the white and black filament samples pieces used for assessing different solvents for smoothing. All samples were approximately from 1 x 1.5 x 0.5 cm^3 to 3 x 0.75 x 0.5 cm^3. Both samples show ridges along the surface.

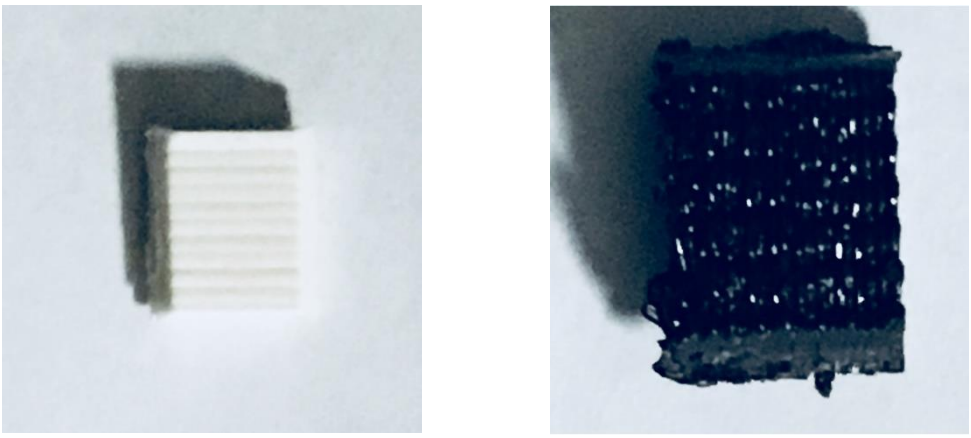

Figure 2.2 Before smoothing images of (left) white PLA sample and (right) black PLA sample. Ridges can be seen along the surface of both samples.

Vaporization was overall better with chloroform and dichloromethane when compared to ethyl acetate, which yielded poor smoothing, as seen in Figure 2.3.

Figure 2.3 PLA samples after vaporization with (left) ethyl acetate, (middle) DCM, and (right) chloroform.

The results from dipping with different solvents is shown in Figure 2.4. Again, the results were more promising with chloroform and DCM than in ethyl acetate, although dipping in ethyl acetate yielded better results than with vaporization.

Figure 2.4 PLA samples after dipping with ethyl acetate (left), DCM (middle), and chloroform (right).

Excessive dipping with any solvent results in deformation of the samples (Figure 2.5). There is an increase in areas with higher melting and imperfections.

Figure 2.5 Examples of excessive dipping with (left) DCM and (right) chloroform.

Figure 2.6 shows vaporization of the black filaments. There was little to no smoothing on the surfaces and a white residue would form on the surface after smoothing.

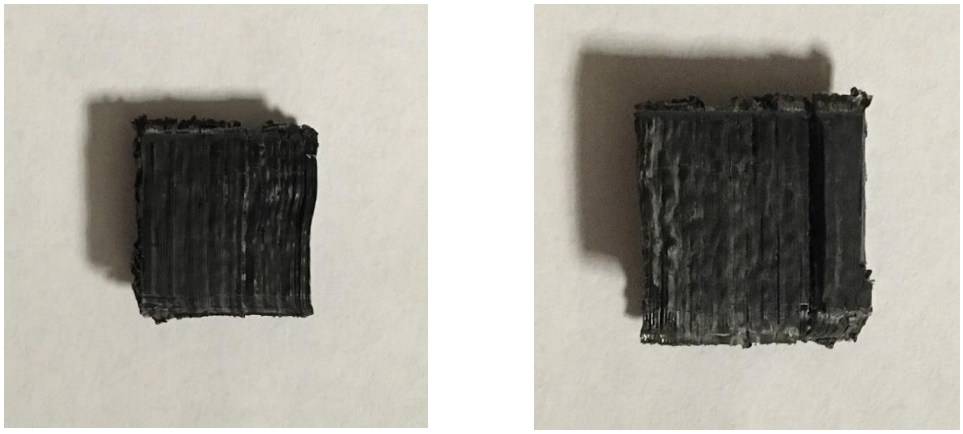

Figure 2.6 PLA samples after vaporization with (left) DCM and (right) chloroform.

The solvent dipping results also showed little to no smoothing of the surfaces (Figure 2.7). The white PLA filament had overall better smoothing post-processing results than the black PLA filament.

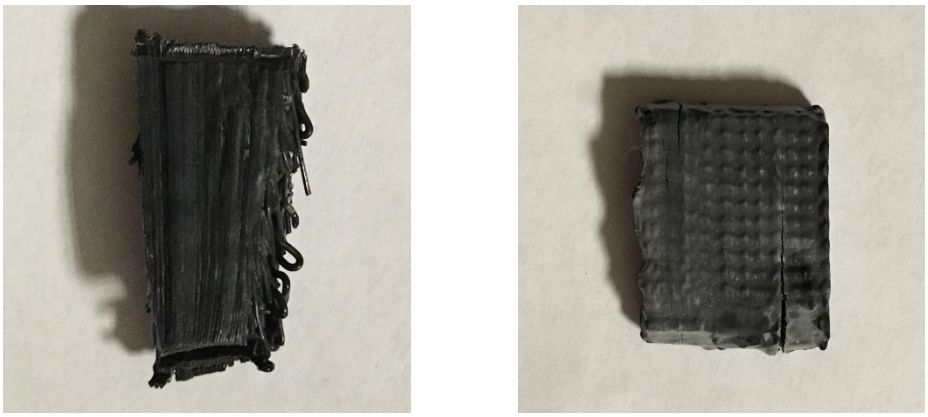

Figure 2.7 PLA samples after solvent dipping with (left) DCM and (right) chloroform.

2.3.2 Design and 3-D printing of capsule circular implants with diameter ≤ 1mm

A test-print (Figure 2.8), which had rows with either a 0.5 mm and 0.3 spacing for each pore size, was made to determine the optimum distance between pores for reducing the filling of pores or merging of open spaces**.** All implants were then printed according to this test print, namely with an inter-pore distance of 33% to 50% of the diameter of the given pore.

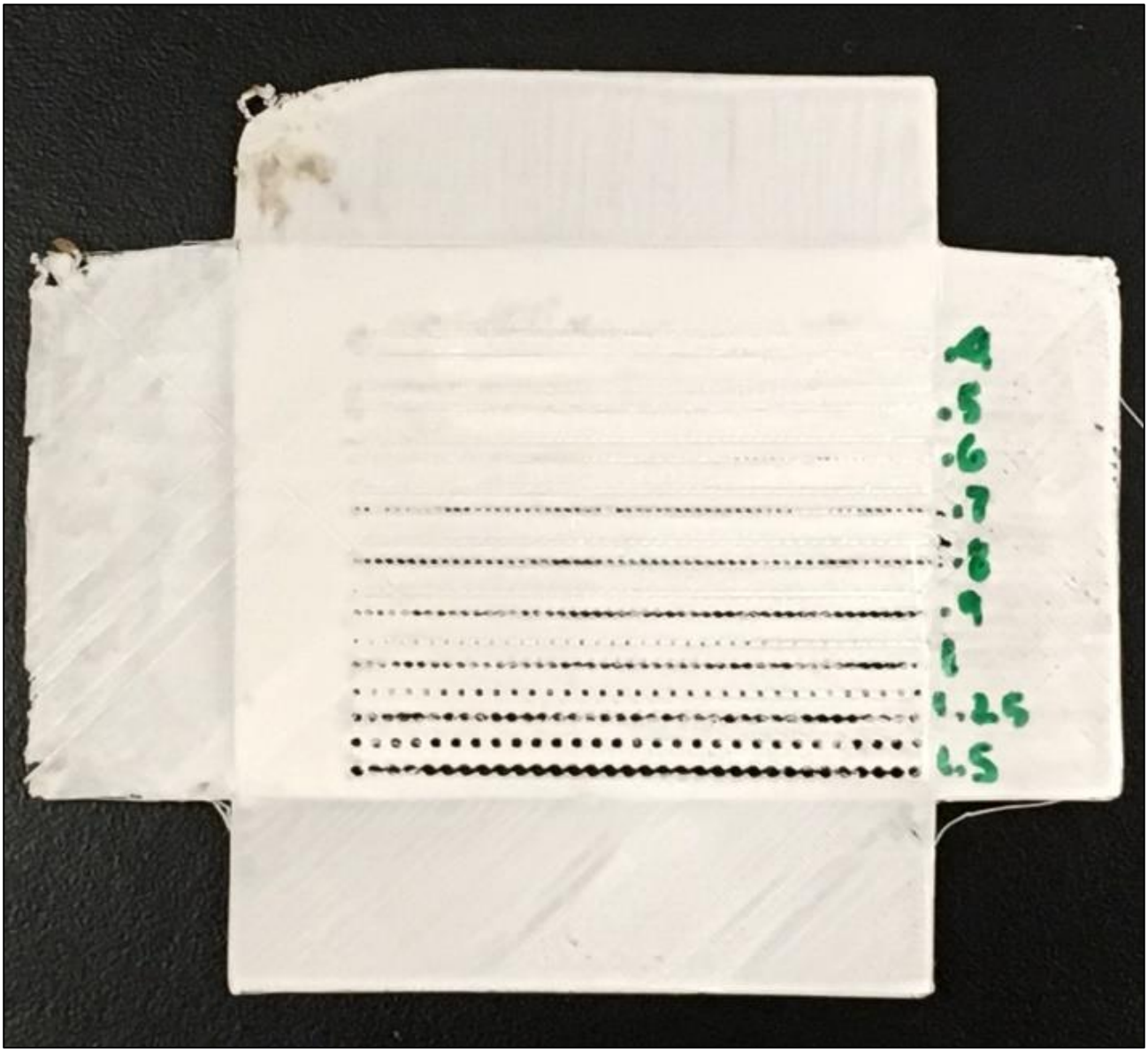

Figure 2.8 Test Print to assess optimum distance for printing between pores. The green markings on the right denote the diameter size (mm) of each pore, each size has two corresponding rows. The top row for each diameter size has an inter-pore spacing of 0.5 mm, while the bottom row has an inter-pore spacing of 0.3mm.

Implants printed with a diameter of 0.6 mm are shown in Figure 2.9. The actual images of the implants show loss in open pores (16%), pore area (76%), and total pore area/surface area (65%) when compared to the original CAD files. Also the pore shape seems more rectangular than circular.

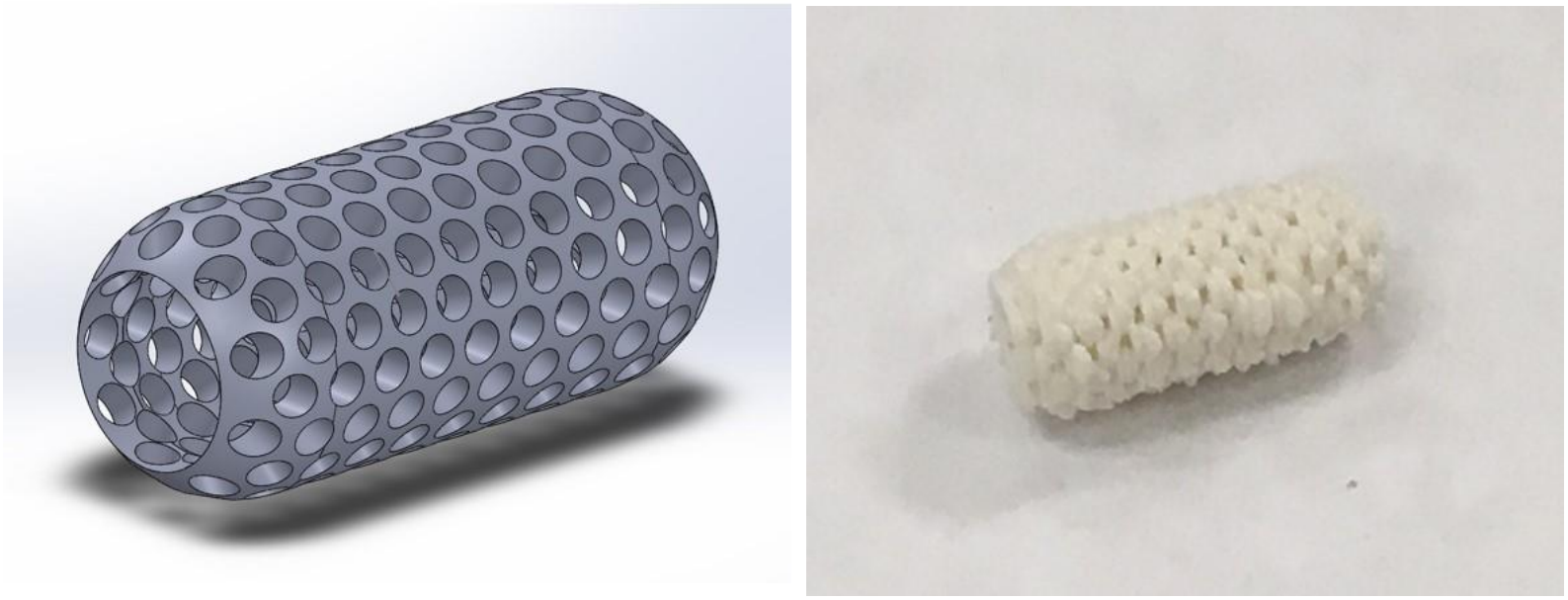

Figure 2.9 CAD design (left) with a 0.6 mm pore diameter and 51.6% total pore area/surface area as well as its actual print (right). The implant had an approximate length of 10 mm, outer diameter of 4 mm, and thickness of 0.5 mm.

Similar results were seen for implants that have a size of 0.8 mm diameter (Figure 2.10). For the 0.8 mm design, there was also a loss in open pores (11%), pore area (84%), and total pore area/surface area (79%) when compared to the original CAD file. The overall shape of both 0.6 and 0.8 mm implants is maintained, but the pore size and total pore area/surface area is reduced due to FDM printing resolution.

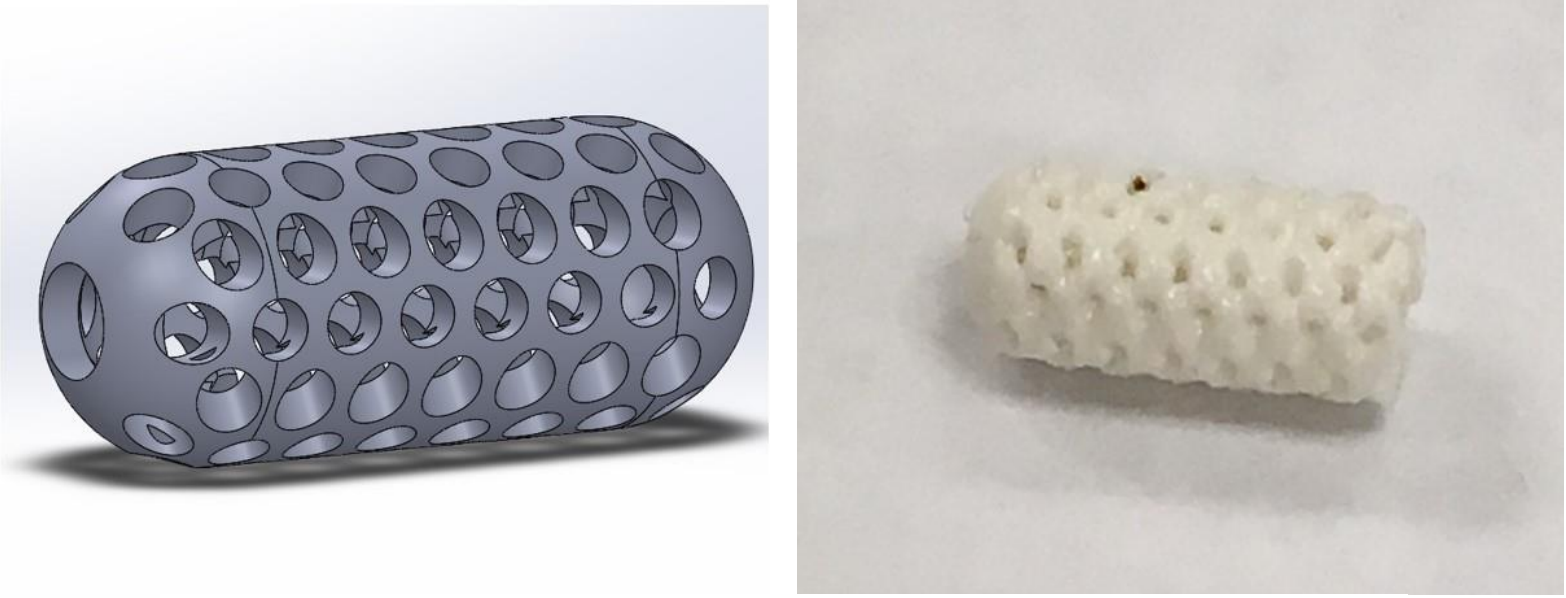

Figure 2.10 CAD design with a 0.8 mm pore diameter and a 38.8% total pore area/surface area as well as its actual print (right). The implant had an approximate length of 10 mm, outer diameter of 4 mm, and thickness of 0.5 mm.

Results for a 1mm diameter implant that received vaporization with chloroform are shown in Figure 2.11**.** The amount of open pores (65%), pore area (78%), and total pore area/surface area (79%) are also highly reduced in the 1mm implant.

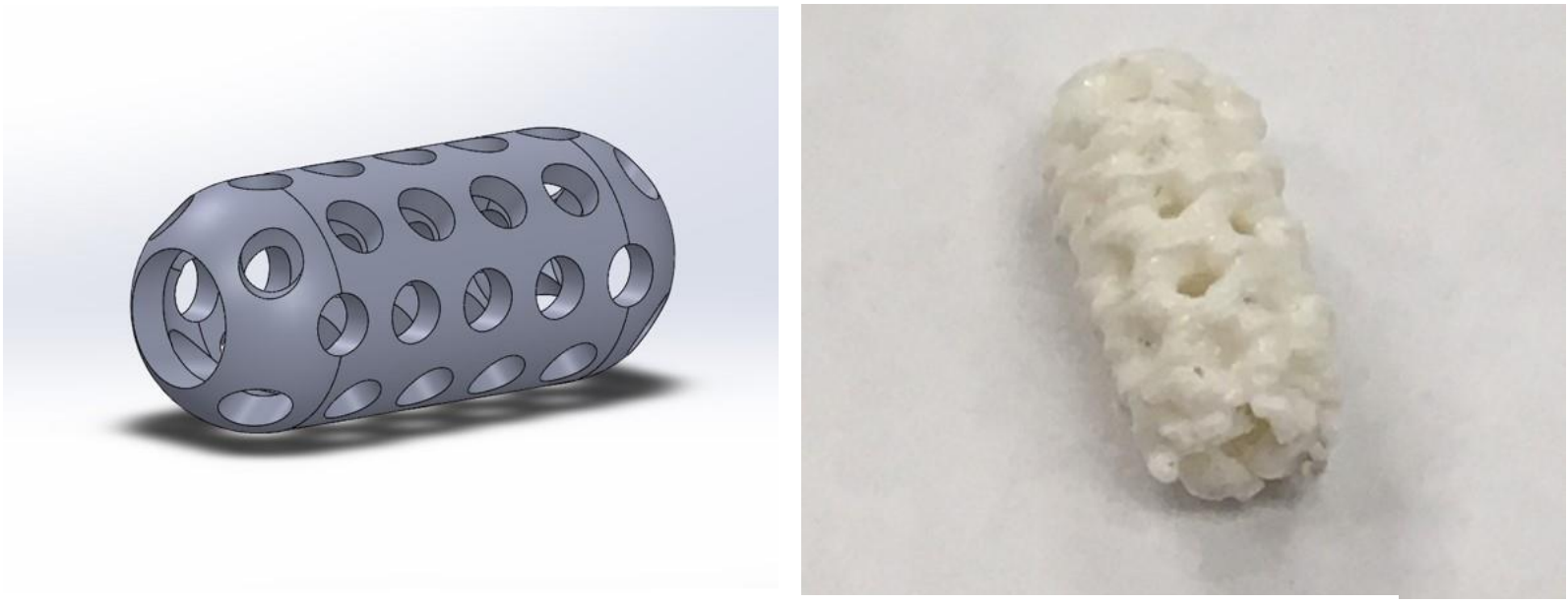

Figure 2.11 CAD design (left) with a 1 mm pore diameter and 41.94% total pore area/surface area as well as its actual print (right). The implant had an approximate length of 10 mm, outer diameter of 4 mm, and thickness of 0.5 mm.

A design of an implant, with drafted holes from 0.9 to 0.6 mm, was printed and processed with chloroform vaporization (Figure 2.12)**.** The results show high reduction in pore area (89%), total pore area/surface area (70%), and number of pores (22%), as well as melting of one end of the implant due to excessive smoothing.

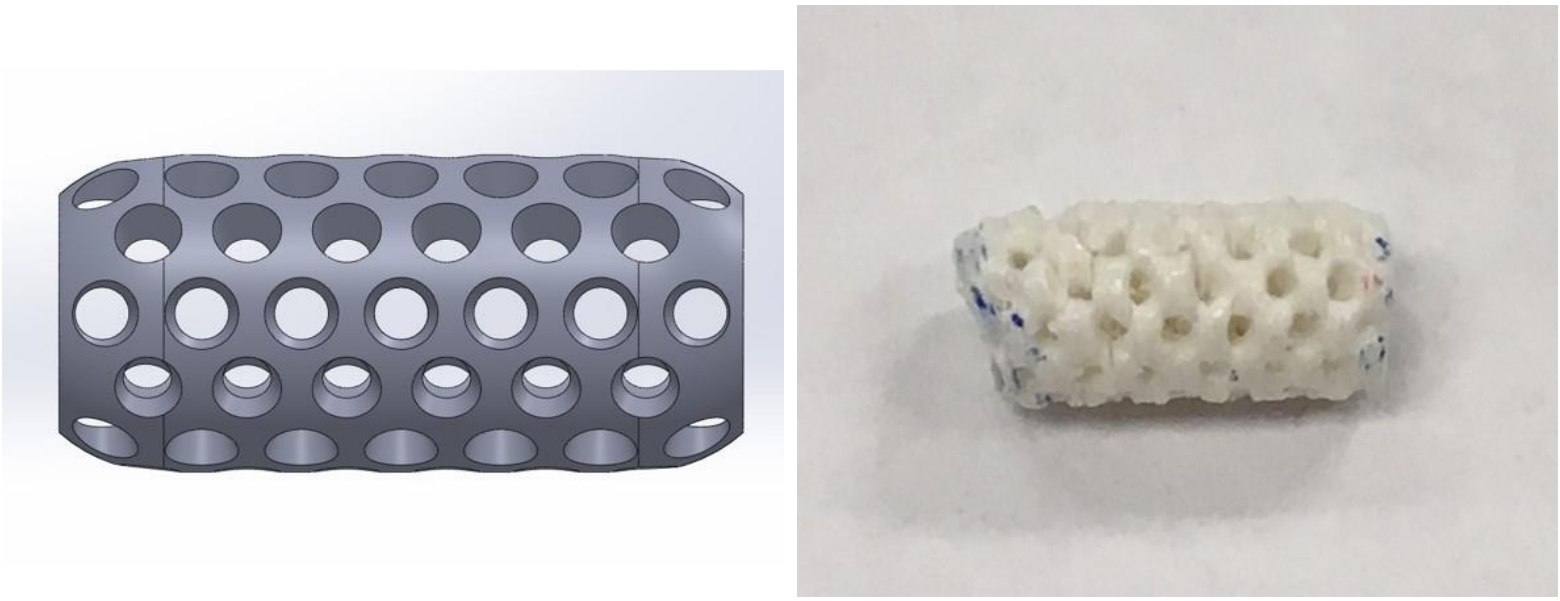

Figure 2.12 CAD design (left) with a 0.9-0.6 mm diameter drafted pore from outer to inner regions and 50.7% total pore area/surface area as well as its actual print (right). The implant had an approximate length of 10 mm, outer diameter of 4 mm, and thickness of 0.5 mm.

The summary of results for the capsule circular implants with a diameter ≤ 1mm is shown in

Table 2.1.

Table 2.1 Summary of results for capsule circular implants with pore diameter ≤ 1 mm

CAD Pore Diameter	0.6 mm	0.8 mm	0.9 mm	1 mm
CAD Pore Area	0.283 mm^2	0.502 mm^2	0.636 mm^2	0.785 mm^2
Actual Pore Area	0.072 mm^2	0.079 mm^2	0.074 mm^2	0.176 mm^2
CAD Total Pore Area/Surface Area	51.6%	38.8%	50.7%	41.94%
Actual Total Pore Area/Surface Area	18.2%	8.10%	14.8%	8.01%
CAD # of Open Holes	191	98	80	46
Actual # of Open Holes	161	87	63	16
% Loss Open Pores	16.0%	11%	22%	65%
% Loss Pore Area	76.0%	84%	89%	78%
% Loss Total Pore Area/Surface Area	65.0%	79%	70%	79%
Shape of Pore	rectangular	circular	circular	circular
Smoothing	No	No	Yes	Yes

2.3.3 Design and 3-D printing of implants with slot design

The total pore area/surface area (83%), pore area (78%), and open pore number (87%) was reduced compared to the CAD design in the smoothened implant with a 0.6-0.5 drafted slot design (Figure 2.13).

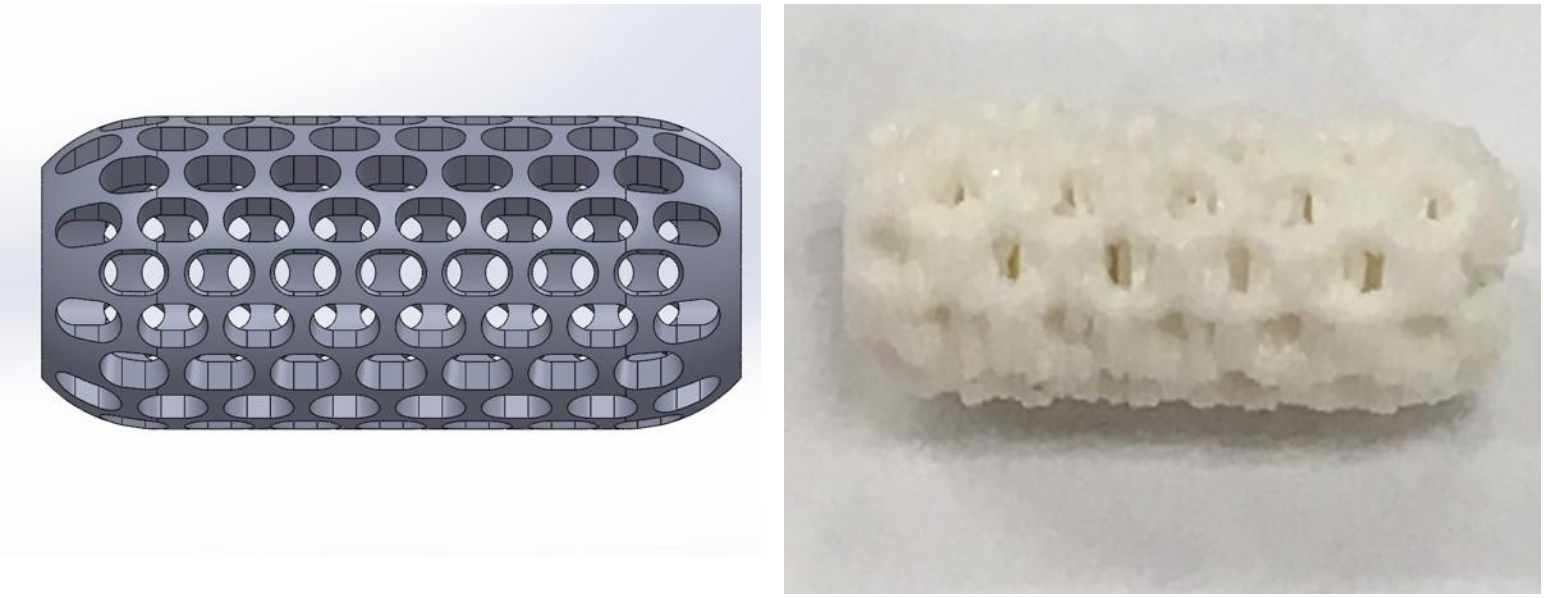

Figure 2.13 CAD design (left) with 0.6-0.5 mm drafted pore diameter and 58.8% total pore area/surface area as well as its actual print (right). The implant had an approximate length of 10 mm, outer diameter of 4 mm, and thickness of 0.5 mm.

A design with a 0.9-0.6 draft (Figure 2.14) was printed with black and white PLA filament. The black filament showed a reduction in total pore area/surface area (72%), pore area (63%), and open pore number (62%) compared to the CAD design. The white filament showed a reduction in total pore area/surface area (80%), pore area (63%), and open pore number (87%) compared to the CAD design.

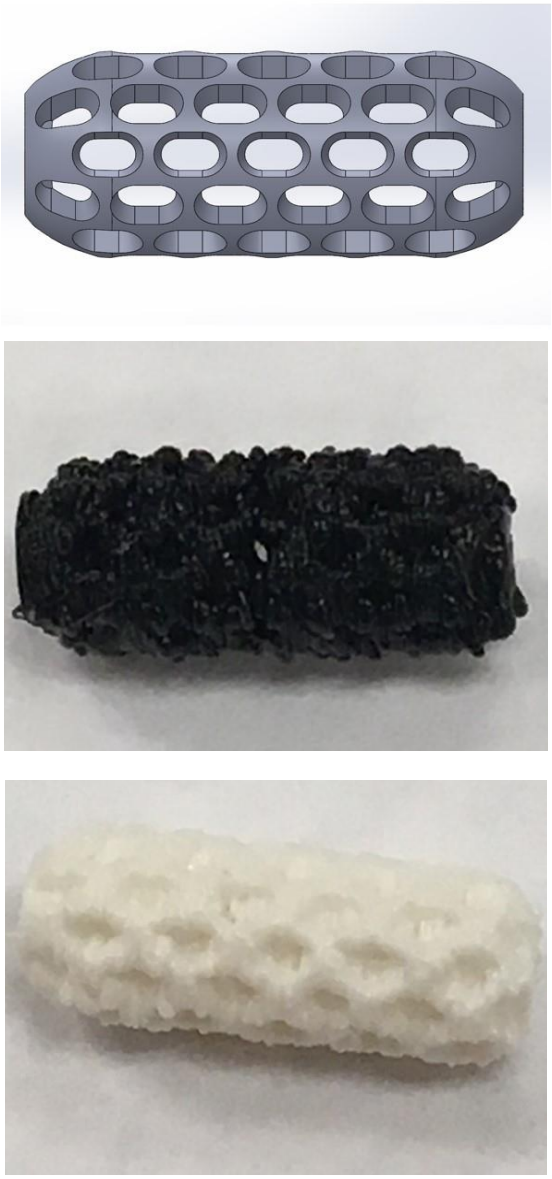

Figure 2.14 CAD design (top) with slot shaped, 0.9-0.6 drafted pores and 65.9 % total pore area/surface area was printed with black PLA filament (middle) and white PLA filament (bottom). The implant had an approximate length of 10 mm, outer diameter of 4 mm, and thickness of 0.5 mm.

The results for the slotted designs are summarized in Table 2.2

Table 2.2 Summary of results for capsule slotted implants

CAD Pore Diameter	0.6 mm	0.9 (Black)	0.9 (White)
CAD Pore Area	0.463mm^2	1.04mm^2	1.04mm^2
Actual Pore Area	0.102mm^2	0.415mm^2	0.388mm^2
CAD Total Pore Area/Surface Area	58.8%	65.9%	65.9%
Actual Total Pore Area/Surface Area	10.5%	19.2%	13.4%
CAD # of Open Holes	137	68	68
Actual # of Open Holes	19	26	9
% Loss Open Pores	87.0%	62%	87%
% Loss Pore Area	78.0%	63%	63%
% Loss Total Pore Area/Surface Area	83.0%	72%	80%
Shape of Pore	Slot-like	circular	Slot-like

2.3.4 Design and 3-D printing of implants with diameter above 1 mm

An implant originally designed to have a diameter of 1.2 mm is shown in Figure 2.15. This implant shows a pore area (91%), open pore amount (24%), and total pore area/surface area (82%) reduction when compared to CAD design after smoothing.

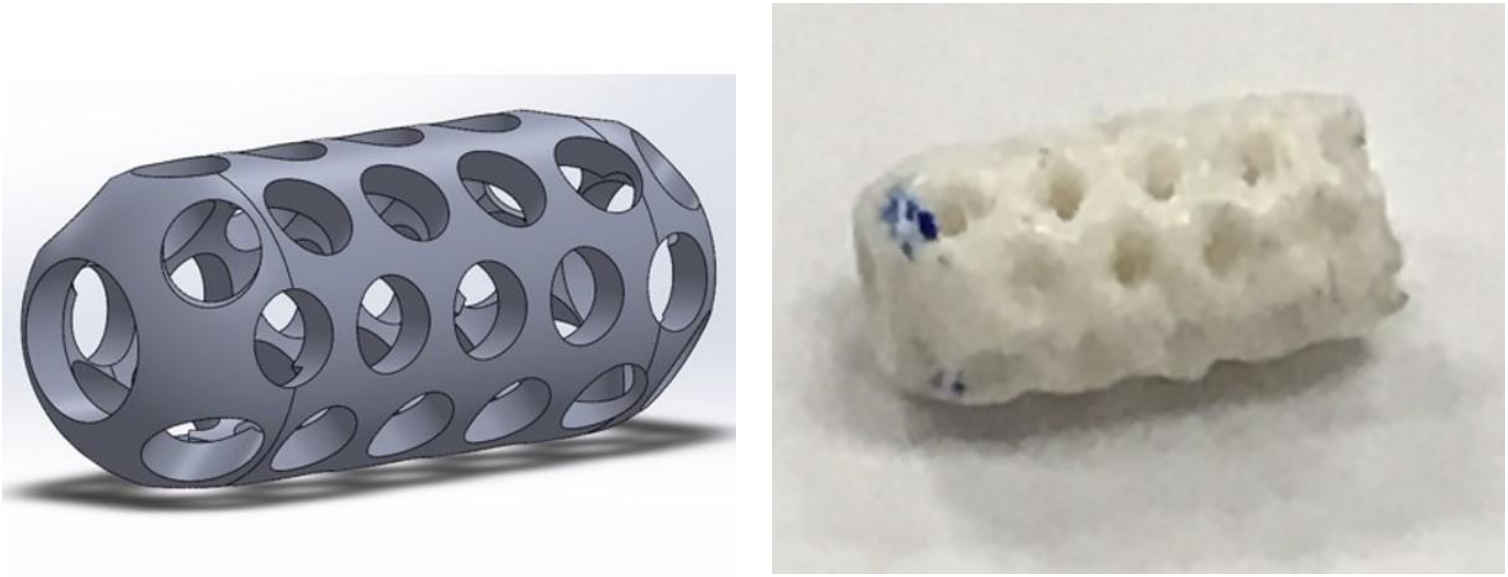

Figure 2.15 CAD design (left) with a 1.2 mm pore diameter and 45% total pore area/surface area as well as its actual print (right). The implant had an approximate length of 10 mm, outer diameter of 4 mm, and thickness of 0.5 mm.

Figure 2.16 shows the CAD design and printed implants for CAD defined pore diameters ranging from 1.4-2.2 mm. The amount of open pores was 100% and the total pore area/surface area was approximate 30% for all these designs. The 1.4 implant showed a 37% total pore area/surface area reduction and 44% pore area reduction, 1.8 showed a 29% total pore area/surface area reduction and 35% pore area reduction, and the 2.2 showed a 15% total pore area/surface area reduction and 18% pore area reduction. Results for the capsule circular implants with pore diameter > 1mm are summarized in Table 2.3.

Figure 2.16 The CAD (left panel) designs are here presented with the respective printed implants (right panel). The designs were specified with a CAD pore diameter of 1.4 (top row), 1.8 (middle row), and 2.2 (bottom row) mm. All implants had an approximate length of 11 mm, outer diameter of 4 mm, and thickness of 0.5 mm.

Table 2.3 Summary of results for capsule circular implants with pore diameter >1mm

CAD Pore Diameter	1.2 mm	1.4 mm	1.8 mm	2.2 mm
CAD Pore Area	1.13mm^2	1.54mm^2	2.54mm^2	3.80mm^2
Actual Pore Area	0.100mm^2	0.863mm^2	1.64mm^2	3.13mm^2
CAD Total Pore Area/Surface Area	45.0%	45.9%	40.0%	35.0%
Actual Total Pore Area/Surface Area	8.10%	28.8%	28.4%	29.6%
CAD # of Open Holes	46	35	18	10
Actual # of Open Holes	35	35	18	10
% Loss Open Pores	24.0%	0%	0%	0%
% Loss Pore Area	91.0%	44%	35%	18%
% Loss Total Pore Area/Surface Area	82.0%	37%	29%	15%
Shape of Pore	circular	circular	circular	circular
Smoothing	yes	no	no	no

2.3.5 Design and 3-D printing of cage-like implants

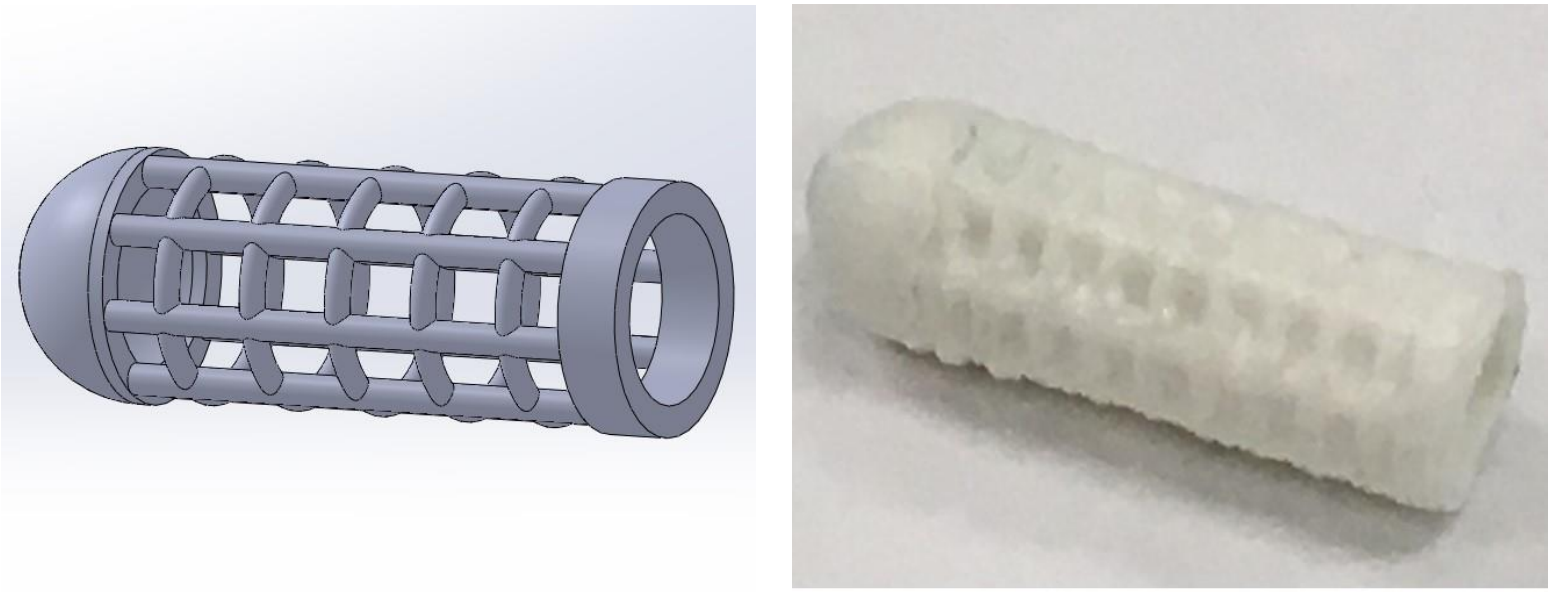

Figure 2.17 CAD design (left) with a 1 x 1.15 mm grate gap and 45 % total pore area/surface area as well as its actual print (right). The implant had an approximate length of 11 mm, outer diameter of 4 mm, and thickness of 0.5 mm.

Implants were printed with a grated design (Figure 2.17), which led to 100% closure of pores, although the outline of the pores and implant was well conserved. Figure 2.18 shows the long gap designs. The 3 Gap implant showed a 26% total pore area/surface area reduction and 46% pore area reduction, 4 Gap showed a 28% total pore area/surface area reduction and 34% pore area reduction, and the 6 Gap showed a 53% total pore area/surface area reduction and 64% pore area reduction. The implants all had an approximate total pore area/surface area of 30% and all of the pores for all implants were open. The results for cage-like designs are summarized in Table 2.4.

CAD Design

Printed Implant

3 Gap

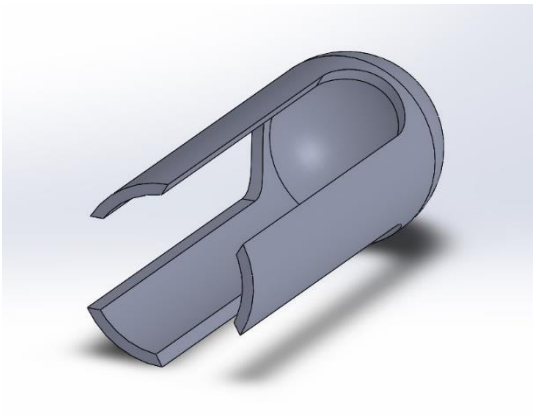

4 Gap

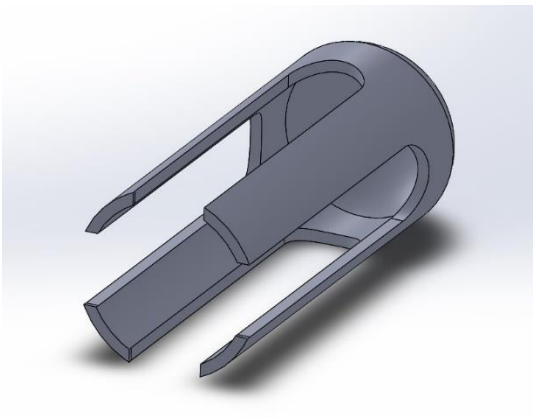

6 Gap

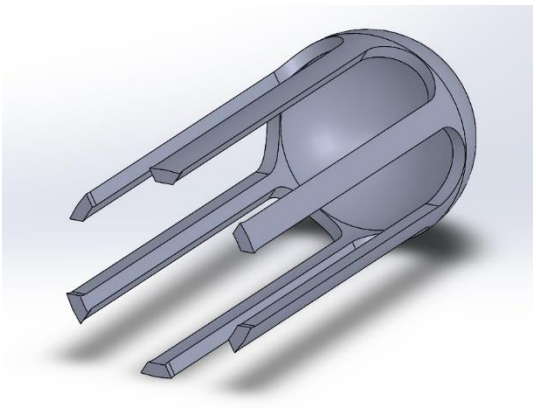

Figure 2.18 The CAD (left panel) designs are here presented with the respective printed implants (right panel). The designs were specified with respect to number of gaps, namely 3 Gap (top row), 4 Gap (middle row), and 6 Gap (bottom row). All implants had a length of 11 mm, outer diameter of 4mm, and 0.5 mm thickness.

Table 2.4 Summary of results for cage-like designs

Design Type	Grate	3 Gap	4 Gap	6 Gap
CAD Pore Area	1.15mm^2	16.9mm^2	12.4mm^2	13.2mm^2
Actual Pore Area	0mm^2	9.09mm^2	8.24mm^2	4.77mm^2
CAD Total Pore Area/Surface Area	45.0%	38.1%	42.8%	60.2%
Actual Total Pore Area/Surface Area	5.0%	28.1%	30.8%	28.0%
CAD # of Open Pores	49	4	5	7
Actual # of Open Pores	1	4	5	7
% Loss Open Pores	98.0%	0%	0%	0%
% Loss Pore Area	100.0%	46%	34%	64%
% Loss Total Pore Area/Surface Area	93.0%	26%	28%	53%
Shape of Pore	Grate	Gap	Gap	Gap
Smoothing	no	no	no	no

2.4 Discussion

2.4.1 Post-processing tests with PLA samples

The post-processing was more efficient with vaporization than with dipping. Although dipping also yielded good results, it was more prone to excessive melting and deformation of the PLA samples. The least efficient solvent was ethyl acetate; it failed to provide smoothing with vaporization and although it provided smoothing with dipping, it required more exposure than the other solvents, which often led to increased melting and deformation. Smoothing results were very similar between chloroform and DCM for both vaporization and dipping. Smoothing with the white filament was much better than with the black filament. Both dipping and vaporization led to poor results with the black filament. A white residue would form on the affected surface and minimal to no smoothing would occur on the rough edges of the PLA samples. Given the results seen with the solvents, both chloroform and DCM had potential to be used for smoothing the implants. In addition, vaporization was the preferred method for smoothing the implants, which were more delicate and less compact than the PLA samples used for smoothing assessment.

2.4.2 Design and 3-D printing of implants with diameter ranging from 0.6 to 1.0 mm

The test print was very helpful in determining the optimal distance between pores to evade open space merging or filling in of pores with filament. There were still technical problems arising when the test print reference was followed, but the level of reproducibility did increase after implementing a distance of one-third to one-half the distance of the diameter between pores. Different printing parameters were changed during the initial 3-D printing

before the optimal parameters were met. The fan speed was changed to a minimum operating speed of 55% and maximum of 75% from a minimum of 40% and maximum of 60%. Namely, by increasing the fan speed the angled projections were more consistent and had less excessive melting, which led to the pores being clogged after the print. This effect of fan speed on inclined struts has also been reported in the literature (Dong et al., 2017). This was mainly important for the first designs that implemented two round ends with open pores for gel injection. The layer height was initially set to 0.2 mm and later set to 0.1 mm. This change did improve the quality of the prints as well, which is not surprising because the majority of the nozzle movements are in the horizontal direction. This latter statement would concur with a study that supported layer height as the main factor that affects the fidelity of horizontal struts (Dong et al., 2017). It also must be noted that different temperatures proved effective for the white and black filaments. Specifically, the white filament extrusion was more effective when the temperature was at 190°C and the black filament extrusion was more effective when the temperature was at 200°C. The initial goal was to make the pores as small as possible and with a high total pore area/surface area as well. The overall pore shape, total pore area/surface area ratio, pore number, and pore area loss in these traps was mainly due to the limitations of FDM, which is usually expected to some degree (Gremare et al., 2017). Designs with a CAD defined diameter of 0.6 and 0.8 were the smallest pore designs that were printed. They both had overall high reductions in total pore area/surface area ratios and 0.6 mm implants had rectangular shaped instead of circular shaped pores. These two implants also did not receive smoothing, so their shortcomings were due to the limitations of FDM. Other parameters

limiting performance that have been reported in the literature includes the effect of printing speed, extrusion flow rate, and nozzle diameter on the layer height (Norman et al., 2017). Since layer height or layer thickness is the main characteristic affecting the fidelity of horizontal struts, these variables become directly related to the printing outcome. For this matter, the printing speed and extrusion flow rate was kept low, at about 10% of total speed for the initial layers to be placed. When the design showed stable printing of the first layers, the speed was then increased by at least 20% and carefully monitored in case issues should arise. Despite the improvement with a slow printing speed for the first layers, there would still be a level of pore reduction due to precision issues during the horizontal strut deposition. Accordingly, it would be a good idea to test the printing with another extruder diameter to see if the pore fidelity could be improved. The design with a 0.9-0.6 mm draft was made to possibly improve the amount of pores that could stay open after printing. The reasoning was that the pores seemed to be closer on the inner cylinder than the outer cylinder when observed in SolidWorks®, so in an effort to maintain the spacing on the inner cylinder as the outer cylinder, the pores were drafted to a smaller diameter. The drafted design was also treated with vaporization and found to have a high reduction in total pore area/surface area. In this case, it was mainly due to reduction in pore area and not number of pores, which was reduced by 22%. Since smoothing led to pore reduction and FDM already led to high pore area reduction within the 0.6-1mm range, smoothing was not considered a good post-processing step to take after printing with designs in this range. Also, since smoothing was only effective with the white filament, no smoothing was attempted on black PLA implants. Overall, the prints had a high total pore area/

surface area ratio reduction ranging from 65 to 79% and the loss in pore area was stable and high as the pore size increased from 0.6 mm to 1 mm.

2.4.3 Design and 3-D printing of implants with slot design

The slot design was made to increase the potential total pore area/surface area of the printed implants. Since pore fidelity is affected by the amount of spacing between pores, which limits the amount of circular pores that can be added, slots, which are defined by two half circles and one center rectangle, were implemented to increase the amount of open space. Indeed, the two best slot designs presented here had the highest CAD design total pore area/surface area ratios of all implants. However, when the designs were printed, their ratios were much lower than in the CAD design. The black and white designs with the 0.9-0.6 draft had great reductions in total pore area/surface area, open pore number, and pore area without smoothing. Even after many trials with this design, the total pore area/surface area could not be increased beyond 20%. In addition, many of the slot designs would often have a high degree of infill within the hollow chamber where the gel is to be placed. The reason for the high degree of failure with this design could be due to parameters set on Slic3r® and the spacing between pores based on the test print. It could be likely that a higher amount of spacing is needed between slots or that a different fan speed and layer height is more optimal for this particular design. A test-print for assessing the optimum distance between slots would be beneficial to unraveling this problem. In addition, a design with a flat end resting on the print bed might provide more stability and aid in the proper printing of the slot shapes.

2.4.4 Design and 3-D printing of implants with diameter above 1 mm

The designs that had a diameter above 1 mm proved to have a higher pore area, total pore area/surface area, and pore number fidelity after printing. The smoothing also went well in terms of open pores in a 1.2 mm implant; however, the pore area reduction was very high (91%). Thus, designs with a 1.2 mm pore diameter are also highly susceptible to high pore reduction after smoothing as designs under 1 mm. Since the aim was to have as high a total pore area/surface area as possible and FDM already has a constant reduction in pore size, smoothing was not attempted with later designs. 3 printed implants, which were derived from designs with a 1.4-2.2 mm CAD diameter size and that had an approximate total pore area/surface area ratio, were selected for assessing their gel retrieval and mechanical properties, which would allow the evaluation of pore size and number on gel retention and retrieval. These three implants also showed 100 % open pore number fidelity, approximately a 30% total pore area/surface area ratio, and a resultant pore area that could be predicted based on the CAD area. A shift from implants with two round ends to one with one round end and one flat end was done to improve printing results, by stabilizing the print in the vertical direction by placing flat end on print bed.

2.4.5 Design and 3-D printing of cage-like implants

The cage-like implants were considered as an alternative to the capsule, porous based designs. They were designed with the idea that they would be easily accessible from the sides of the implant besides the injection port end. The initial designs were defined by an array of

gratings, which would allow easier retrieval access for the gel and still render enough surface tension on the gel so that it stays inside. However, the pore area and open pore number was always close to or equal to zero. Many of the failed attempts had a good outline of the implant and gratings, but the gratings were always filled with filament. When the focus switched to the long gaps cage designs, the results were more promising and comparable to the best capsule based designs. Specifically, all the gaps were open in each long gap design variation and the highest total pore area/surface ratios attained were approximately 30%. It should be noted, however, that the cage-like designs were much harder to print than the capsule based designs. Namely, it required more trials to successfully print on cage-like when compared to capsule designs. This is likely due to the instability in the z-axis due to less support while it prints and due to less cohesive layers in the z-axis. Accordingly, it was surmised that the capsule based designs would be more resistant to mechanical stresses. Also, while both the 3 Gap and 4 Gap designs had low total pore area/surface area reductions of 26% and 28%, the 6 Gap design had a reduction of 53%. This was likely due to higher printing instability in the z-axis, which was observed more in the 6 Gap design versus the other two designs. The three long gap designs with an approximate total pore area/surface area of 30% were selected for assessment of their mechanical and gel retrieval properties. In this way, the cage-like design could be compared with the capsule and the effect of gap numbers on mechanical properties and gel retrieval.

Chapter 3

Mechanical Characteristics

3.1 Rationale

The Von Mises distribution and potential displacement of the two designs, capsule and cage-like, were assessed. All implants were first computationally assessed with a compressive pressure of 0.06 psi based on previous publications, which have reported an average resting pressure value of 0.8 and 3 mmHg from calf and forearm subcutaneous tissue (Olszewski et al., 2010; Wells et al., 1938; Meyer & Holland, 1932; Holland & Meyer, 1932). The characteristics evaluated were the radial Von Mises (N/m^2) and displacement (mm) distributions. The Von Mises distribution is important for assessing the compressive strength due to design and the displacement of different parts of the implants will lead to gel being squeezed out. The median Von Mises and displacement were used to test for significance between capsule and cage-like designs since the median distribution was relatively constant among all designs. Also, one capsule design and one cage-like design were selected for mechanical testing with a uniaxial compression testing machine to determine the elastic modulus. Since dissimilar physical properties are expected due to differences in extruder head printing paths between capsule and cage-like designs, the calculated elastic modulus for each design can shed more light on this relationship.

3.2 Methods

3.2.1 Implants assessed for computational assessment

The capsule implants assessed were the 1.4, 1.8, and 2.2 mm designs that were renamed Capsule-1, Capsule-2, and Capsule-3. The cage-like implants assessed were the 3 Gap, 4 Gap, and 6 Gap designs that were renamed Cage-1, Cage-2, and Cage-3. The implants were designed with the traits shown after printing, that is, with the average pore and gap areas obtained post-printing for all pores and gaps in the CAD designs. They all had an approximate total pore area/surface area ratio of 30%. Their properties are summarized in Table 3.1 and illustrated in Figure 3.1 and Figure 3.2.

Table 3.1 Characteristics of capsule and cage-like implants for mechanical testing

Design	Capsule			Cage-like		
New Name	Capsule-1	Capsule-2	Capsule-3	Cage-1	Cage-2	Cage-3
Previous Name	1.4 mm	1.8 mm	2.2 mm	3 Gap	4 Gap	6 Gap
Pore Area	0.863mm^2	1.64mm^2	3.13mm^2	9.09mm^2	8.24mm^2	4.77mm^2
Amount of Pores	35	18	10	4	5	7
Total Pore Area/Surface Area Ratio	28.8%	28.4%	29.6%	28.1%	30.8%	28.0%

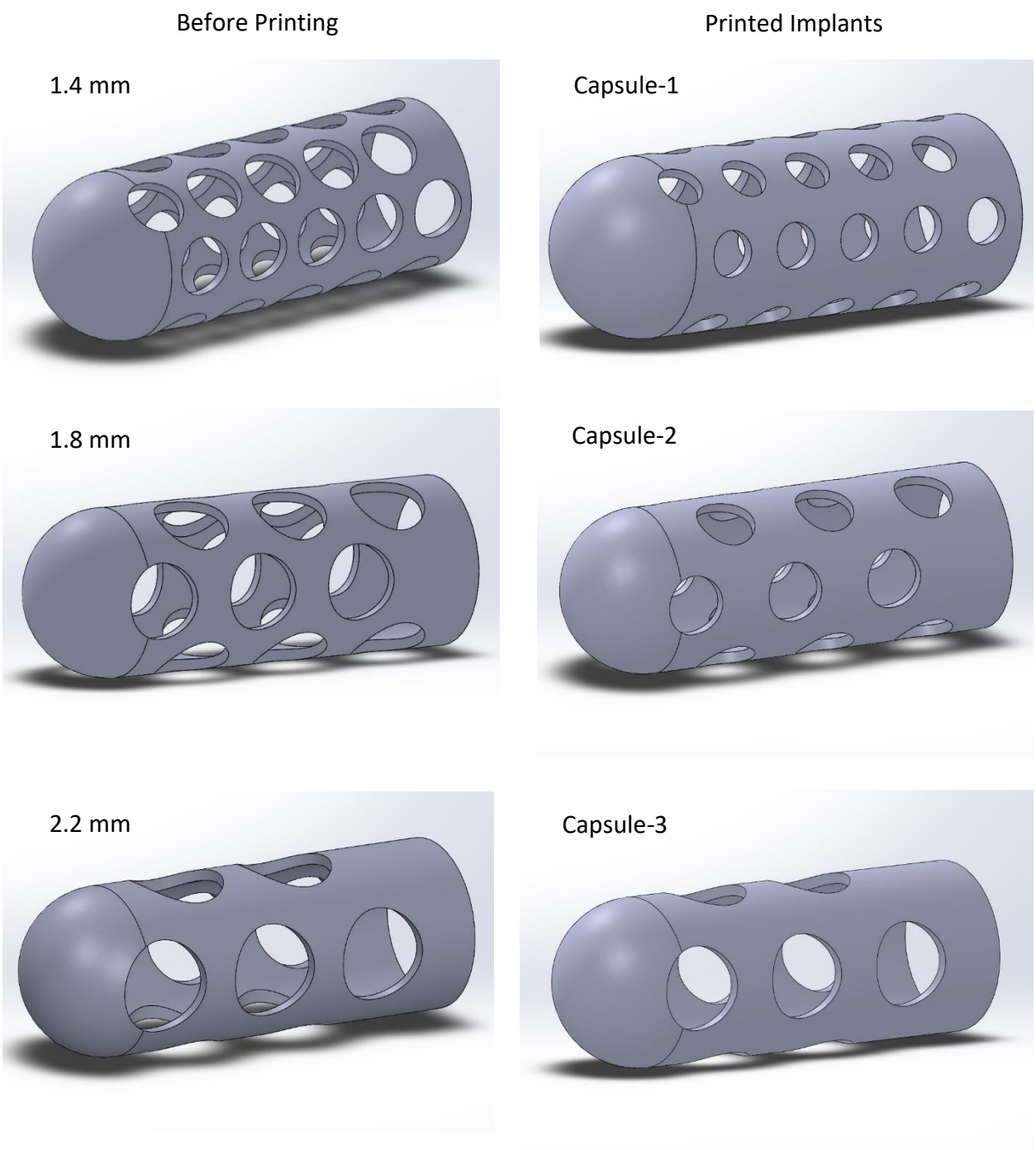

Figure 3.1 The before printing CAD designs (left panel) are here presented with the CAD designs of the printed capsular implants (right panel) used for computational assessment. All implants had an approximate length of 11 mm, outer diameter of 4 mm, and thickness of 0.5 mm, they differed only in terms of pore diameter, which was reduced in printed CAD designs. The names of the implants are denoted in the top left corner of each image.

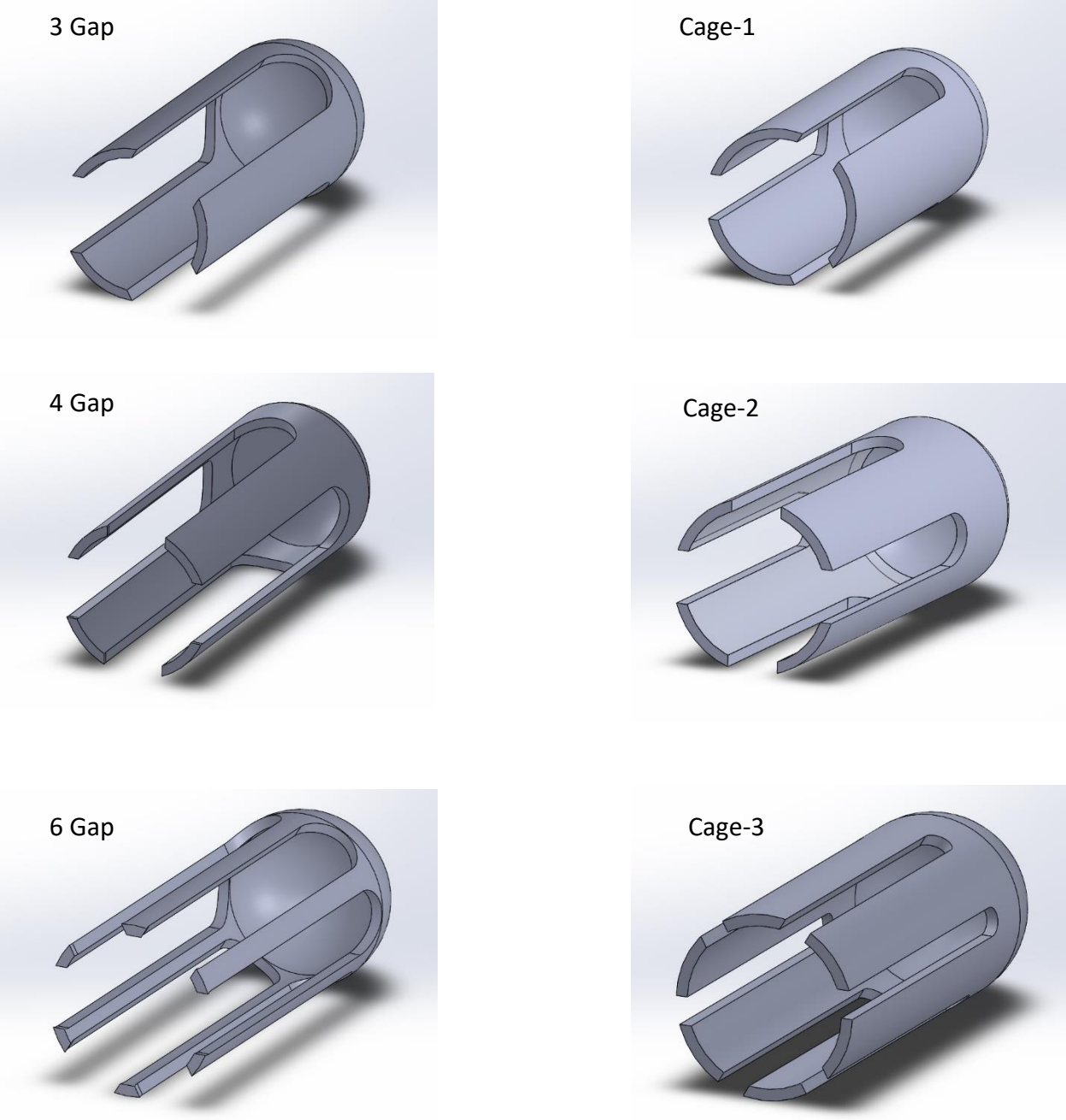

Figure 3.2 The before printing CAD designs (left panel) are here presented with the CAD designs of the printed cage-like implants (right panel) used for computational assessment. All implants had an approximate length of 11 mm, outer diameter of 4 mm, and thickness of 0.5 mm, they differed only in terms of gap size, which was reduced in printed CAD designs. The names of the implants are denoted in the top left corner of each image.

3.2.2 Characterization of PLA on SolidWorks® and compressive assessment

The material properties for lactic acid were characterized on SolidWorks® software: elastic modulus of 3.5 x 10^9 N/m^2, poisson's ratio of 0.36, mass density of 1249.44 kg/m^3, and compressive strength of 93,000,000 N/m^2. Modeling of compressive forces was done on SolidWorks® software add-in SimulationXpress. Implants were assessed under a pressure of 0.06 psi and the respective Von Mises and displacement results were used for comparison between capsule and cage-like designs.

3.2.3 Compression mechanical testing

A mechanical testing machine, MTS Insight Electromechanical-2kN®, was used to assess compression testing in the axial axis. Capsule-2 (n=3) and Cage-3 (n=3) were tested under an initial compression force of 0.18 N and extension rate of 1.65 x 10^{-3} mm/ sec. The extension and force was increased until mechanical failure. The compression tests were conducted at 23° C. The implants were placed in a vertical position so that the compression was rendered axially. The engineering stress and strain were used to define the stress-strain plot.

3.2.4 Statistics

All statistical calculations were done on Microsoft Excel 2017.The student's t-test was used to calculate significant differences in median Von Mises and displacement between cage-like and capsule designs. The cage-like designs assessed were Cage-1, Cage-2, and Cage-3. The capsule designs compared were Capsule-1, Capsule-2, and Capsule-3.

3.3 Results

3.3.1 Computational assessment

When comparing all capsule (n=3) and cage-like (n=3) designs in terms of median Von Mises, the difference was significant ($p<0.05$), as shown in Figure 3.3.

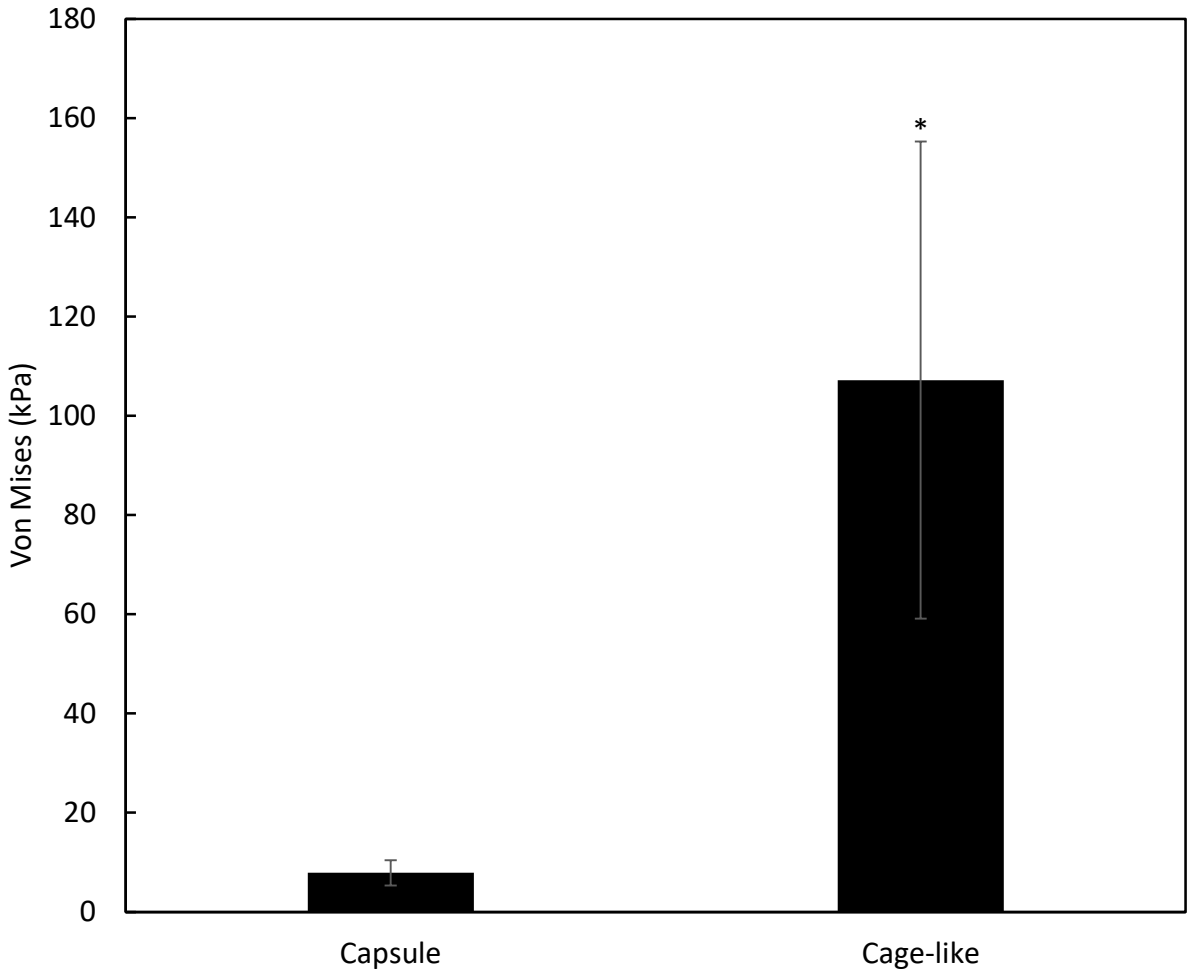

Figure 3.3 Median Von Mises rendered on capsule (n=3) and cage-like (n=3) designs due to 0.06 psi compressive pressure. Significance was determined at $p<0.05$ *, $p<0.01$**

When comparing all capsule (n=3) and cage-like (n=3) designs in terms of median displacement, the difference was significant ($p<0.05$), as shown in Figure 3.4.

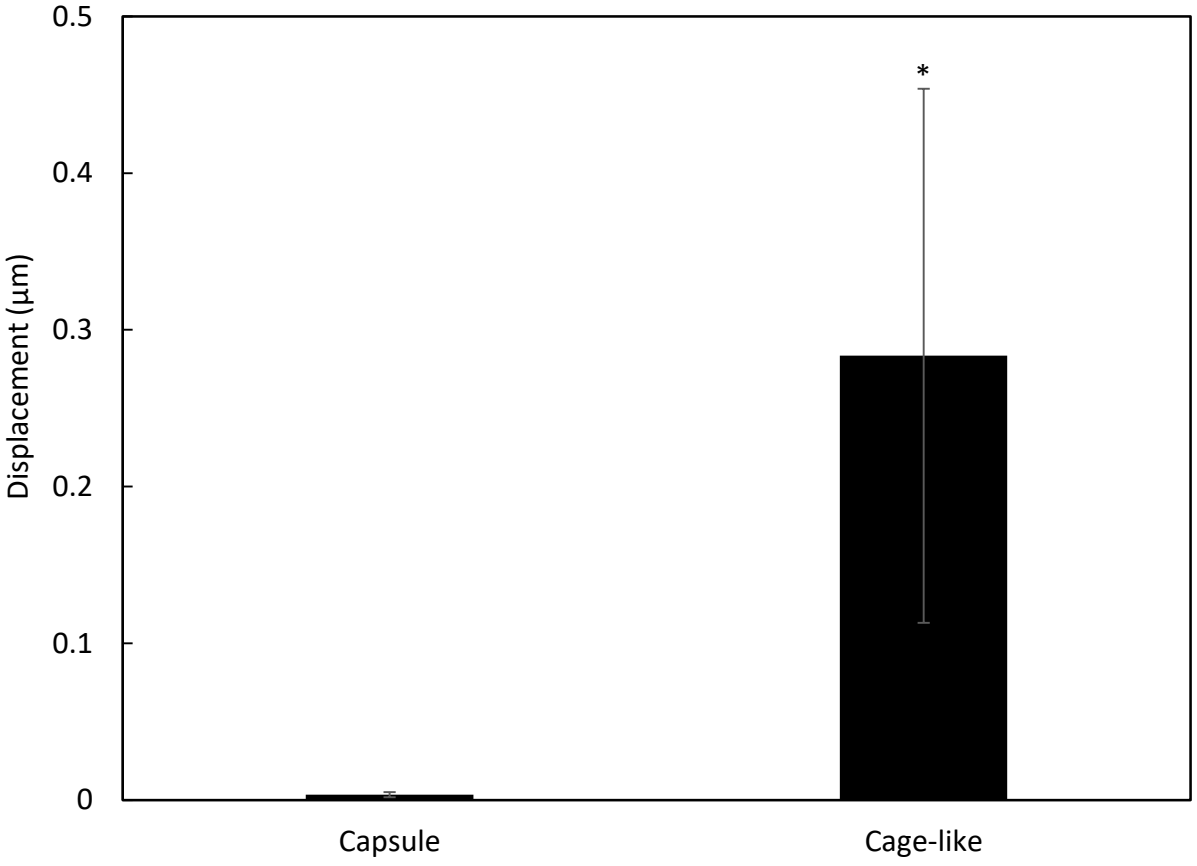

Figure 3.4 Median displacement rendered on capsule (n=3) and cage-like (n=3) designs due to 0.06 psi compressive pressure. Significance was determined at $p<0.05$ *, $p<0.01$**

The results from the computational compression tests are summarized in Table 3.2.

Table 3.2 Median Von Mises and displacement from computational pressure assessment

Design	Von Mises (kPa)	Displacement (μm)
Capsule-1	6.088	0.0029
Capsule-2	6.788	0.0021
Capsule-3	10.81	0.0052
Cage-1	71.35	0.1496
Cage-2	88.39	0.2256
Cage-3	161.8	0.4753

3.3.2 Compressive mechanical testing

Based on the stress-strain curve (Figure 3.5) derived from the Capsule-2 mechanical testing data, the elastic modulus for capsule implants was estimated at 7794.9 ± 1119.6 kPa and its yield point at 0.2 % offset at 25097 ± 2795.4 kPa. Its proportionality limit was reached at 2% strain and its yield point at 4% strain.

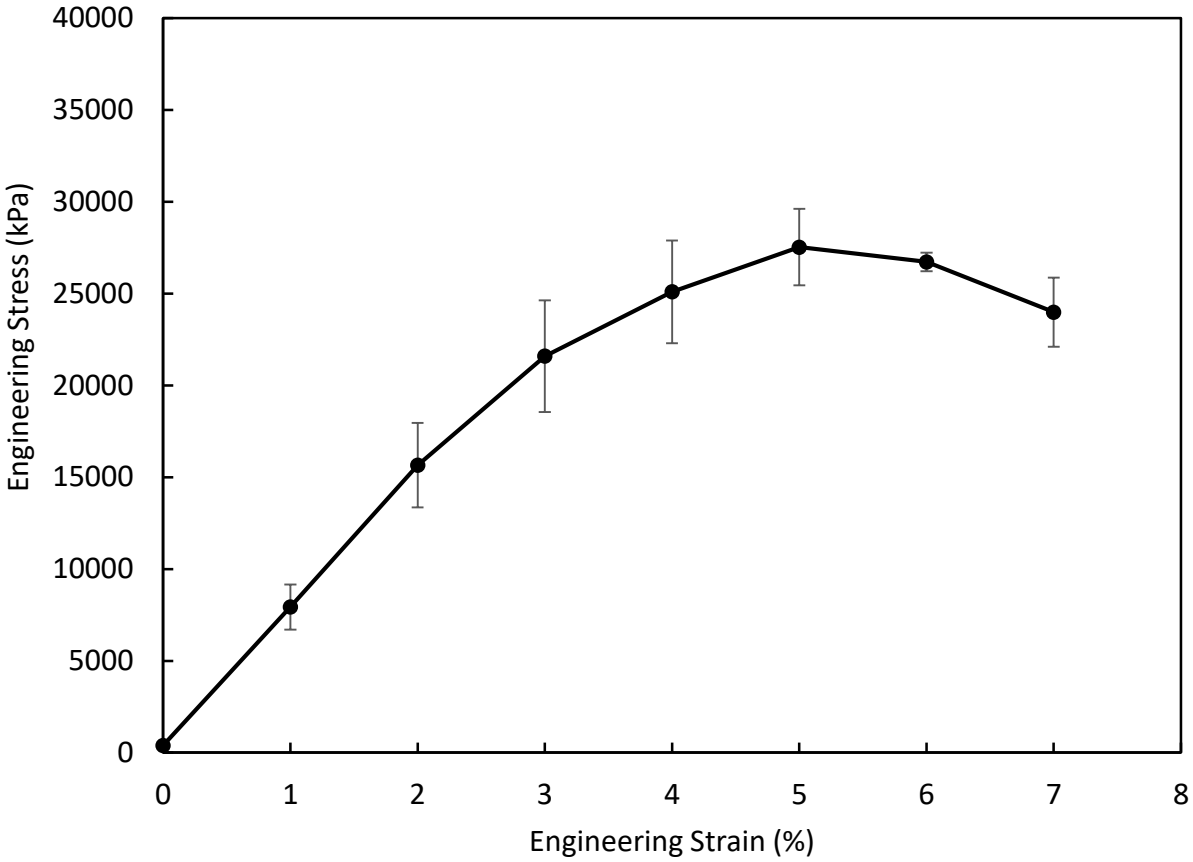

Figure 3.5 Stress-strain plot of Capsule-2 implants (n=3) under uniaxial compression.

The elastic modulus for Cage-3 was determined to be 21953 ± 4895.46 kPa and its yield point at 0.2% offset at 39521 ± 9192.6 kPa (Figure 3.6). Its proportionality limit was reached at 1% strain and its yield point at 2% strain.

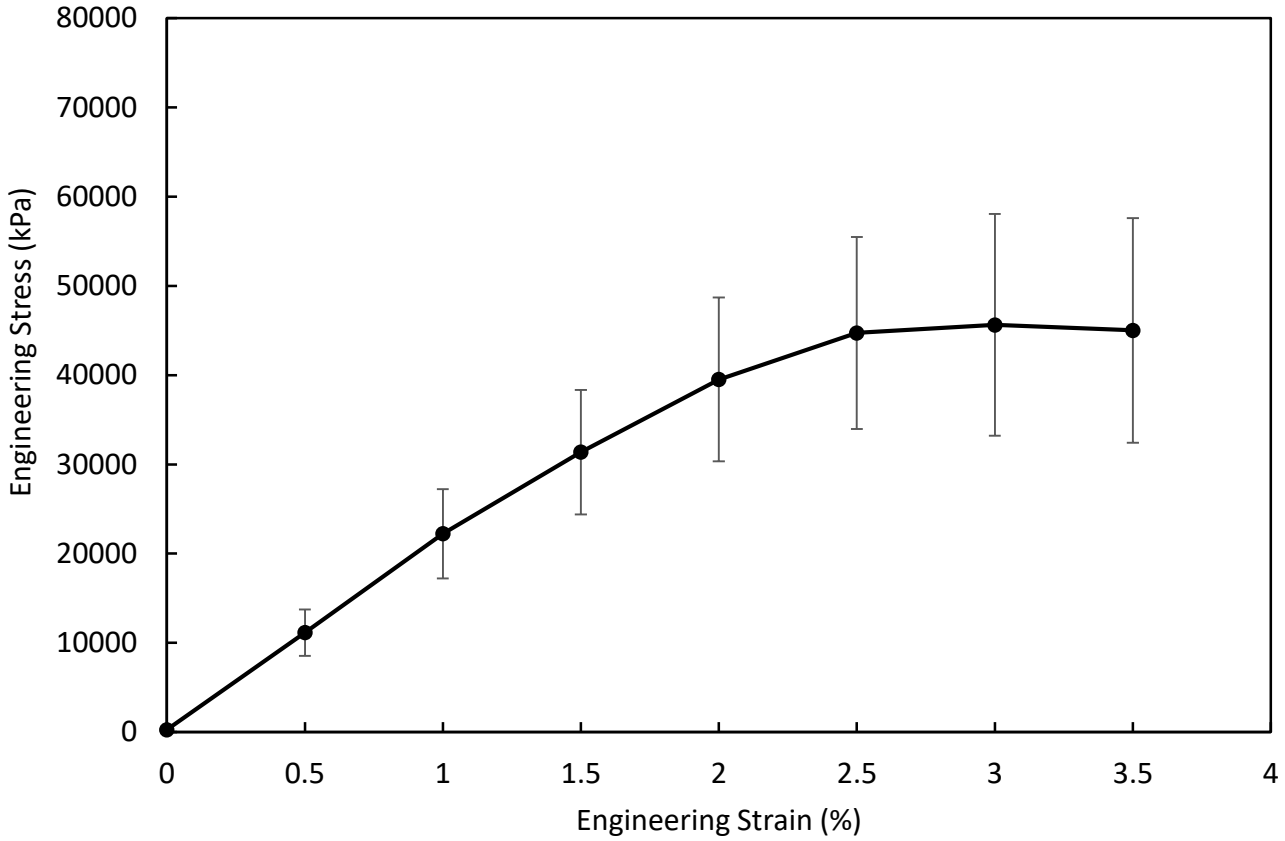

Figure 3.6 Stress-strain plot of Cage-3 implants (n=3) under uniaxial compression.

Table 3.3 shows the mechanical properties calculated for Capsule-2 and Cage-3.

Table 3.3 Mechanical properties of implants

Design	Capsule-2	Cage-3
Elastic modulus	7794.9 ± 1119.6 kPa	21953 ± 4895.46 kPa
Yield point	25097 ± 2795.4 kPa	39521 ± 9192.6 kPa
Strain where proportionality limit reached	2%	1%
Strain where yield point reached	4%	2%

3.4 Discussion

3.4.1 Computational Assessment

The Von Mises analysis shows that all capsule and cage-like implants can be placed in subcutaneous tissue without any risk of the stress producing plastic deformation. Thus, capsule and cage-like implants should not experience mechanical failure while in subcutaneous tissue. In this way, the main factor affecting degradation of the implant would be hydrolysis. The Von Mises was higher ($p<0.05$) in cage-like than in capsule designs, likely due to its geometric shape with large gaps in the center, which makes it less compact than capsule. However, even though it is significantly higher, both implants should not have mechanical failure issues if placed in subcutaneous tissue. The displacement comparison showed a significant difference ($p<0.05$), but the displacement was quite low, namely it was 0.003 ± 0.002 μm for capsule and 0.284 ± 0.170 μm for cage-like designs, so there should be minimal to no displacement. Even though with PLA the displacement and Von Mises distributions will not cause gel leakage or mechanical failure, a weaker material might collapse and leak gel with the given designs. The purpose of the comparison between cage-like and capsule designs was to assess how the design changes the mechanical properties, which would facilitate the selection of a design given a certain material.

3.4.2 Compressive mechanical testing

Even though the elastic modulus is a property of the material and not structure, different printing parameters in FDM, such as layer thickness, position on print bed, and

temperature, can lead to differences in mechanical properties of the material, irrespective of structure (Kundera & Bochnia, 2014; Kundera & Kozior, 2014; Adamczak, Zmarzly, & Stepien, 2016). These parameters mainly affect the microstructural anisotropy caused by the layer-by-layer manufacture process (Christiyan, Chandrasekhar, & Venkateswarlu, 2016). The effect of printing parameters has been related to compressive strength (Sood, Ohdar, & Mahapatra, 2012). Furthermore, a recent study by Kozior & Kundera (2017) that examined the effect of printing orientation on the elastic modulus of approximate 10 mm ABS cylindrical samples supported different resultant elastic moduli for different orientations. Based on these previous experiments with FDM, it was surmised that if differences in the layer cohesiveness were to occur due to differences in how the capsule and cage-like designs are printed, then the elastic modulus will change. The assessment was on the integrity of the layers as they were printed in the z-axis and not on the geometrical structure of the two designs. Accordingly, it has been reported in the literature that the influence of layer thickness and bond stability between layers in the z-axis affects the mechanical integrity in 3-D printed objects (Kuznetsov et al., 2018). As predicted, the cage-like designs showed a higher elastic modulus (21953 ± 4895.46 kPa) when compared to capsule designs (7794.9 ± 1119.6 kPa). The capsule designs normally required less operator intervention, specifically less adjustment of temperature, extruder height, and printing speed. The cage-like, on the other hand, required more monitoring and adjustment of these said parameters. Extruder height was likely the most important parameter that caused differences in elastic modulus, as it was the parameter most often manipulated. Indeed, if the extruder height was too high both the capsule and cage-like designs had a very weak

mechanical structure that could be easily broken apart. Since the main adjustment in cage-like was to make sure that the extruder height was as low as possible while still permitting printing, it is likely that the layers were more compactly printed. Specifically, a layer that is more compressed should create more surface area on the X/Y plane, which would then lead to higher contact area and higher layer adhesion. This would then lead to a stronger compressive strength in the z-axis. Accordingly, the radial compressive strength should not be as increased as the axial compressive strength, which is likely why there was a higher Von Mises in the Cage-3 design versus Capsule-2 during computational assessment. In addition, the computational assessments do not take into account the effect of layer cohesiveness rendered by printing, which could lead to different elastic moduli and results for both capsule and cage-like designs. Nevertheless, both Capsule-2 and Cage-3 showed mechanical properties that are highly suitable for the physiological pressures found in subcutaneous tissue. To further assess the effect of the layer cohesiveness on elasticity and compressive strength, it would be ideal to compare the same capsule or cage-like design with different axial layer integrity rendered by different extruder heights. These observations serve to guide the optimization of the mechanical properties of 3-D printed subcutaneous implants to improve their medical applications. This latter statement is supported by a study that assessed different elastic moduli and yield stress values of a hydrogel in a rodent subcutaneous model, which led to varying levels of performance, such as life-time and vascularization, as mechanical properties were changed (Pilipchuk et al., 2013). A weaker material for 3-D printing than PLA would likely need careful tailoring of its mechanical characteristics.

Chapter 4

Gel Retrieval

4.1 Rationale

The ability to retrieve gel from the most optimal capsule and cage-like implants were evaluated to determine the most efficient implant. All implants compared here had an approximate total pore area/surface area of 30% to evaluate the effect of design and pore size or gap number on the ability of the implants to retain and allow retrieval of gel. The implants were first assessed on their ability to retain gel and allow retrieval while placed on a paper towel. They were then compared while in a gelatin and agar based phantom tissue, which has been shown to provide an accurate model of hypodermis layers (Chen et al., 2016). In this way, it is feasible to deduce if gel is lost due to the physical properties of the implant, delivery method, or interaction of implant with phantom tissue. The most optimal implant from these studies was then used to create the final prototype for testing gel retrieval from murine subcutaneous space. Namely, it was designed exactly the same way except for its total side length, which was changed from 9 to 13 mm. The implants were delivered to the inner phantom tissue space and murine subcutaneous space via a trocar based device. This device has been used clinically and is the favored delivery method since it allows proper placement of cylindrical objects after a tunnel is created with the metal part of the trocar.

4.2 Methods

4.2.1 Implants Assessed

The capsule implants assessed for retrieval from phantom tissue were the 1.4, 1.8, and 2.2 mm designs that were renamed Capsule-1, Capsule-2, and Capsule-3. The cage-like implants assessed were the 3 Gap, 4 Gap, and 6 Gap designs that were renamed Cage-1, Cage-2, and Cage-3. Their denominations are summarized in Table 4.1. They all had an approximate total pore area/surface area of 30%. The most efficient design was then used to make the final prototype; that is, the pattern of pores and CAD diameter were kept the same but the total length was increased from 11 to 15 mm and a higher CAD total pore area/surface area was attempted. A control group with the same length and diameter as final prototype but with no pores except for the injection port was also printed to be used in the subcutaneous space assessment.

Table 4.1 Characteristics of capsule and cage-like implants for gel retrieval

Design	Capsule			Cage-like		
New Name	Capsule-1	Capsule-2	Capsule-3	Cage-1	Cage-2	Cage-3
Previous Name	1.4 mm	1.8 mm	2.2 mm	3 Gap	4 Gap	6 Gap
Pore Area	0.863mm^2	1.64mm^2	3.13mm^2	9.09mm^2	8.24mm^2	4.77mm^2
Amount of Pores	35	18	10	4	5	7
Total Pore Area/Surface Area Ratio	28.8%	28.4%	29.6%	28.1%	30.8%	28.0%

4.2.2 Gel Retrieval

A P200 micropipette was used for all gel injections and retrievals. The gel used was hyaluronic acid (HA) with a molecular weight of 700 kDa and a concentration of 20 mg/ml. The phantom tissue used was comprised of 8% Gelatin-1% Agar-0.24% formaldehyde. The phantom tissue was evenly allocated in a 6-well plate. A trocar device with a 4.5 mm inner diameter cannula, metal trocar, and stem was used to place the implants inside the phantom tissue and murine subcutaneous space. A surgical knife was also used for making an incision in the skin of a dead mouse to allow placement of the trocar device. The implant used as the experimental group for retrieval from the dead mouse was the implant that achieved the most gel retrieval percentage from the implant alone and phantom tissue.

a. retrieval from implant alone

A 1.5 ml Eppendorf was weighed on a OHAUS® GA200D scale, set to 4 significant digits, and the resulting weight was then tared. A visual reference for 75 µl was created by dispensing 75 µl of water in a 1.5 ml Eppendorf. Gel was then dispensed in the previously tared Eppendorf until it matched the water filled Eppendorf as closely as possible. The gel-filled Eppendorf was then placed on the scale and the weight recorded. The gel was then injected into the implant, which was left to incubate for 3 minutes on a paper towel. Meanwhile, the residual gel, if any, remaining in the Eppendorf was weighed on the scale. Any observations related to gel leakage from the implant unto the paper towel and injection were recorded. After the 5-minute incubation, the gel was carefully retrieved from the implant and placed into the Eppendorf. The

weight was then recorded and the residual gel was subtracted from the initial and final gel weights. Any observations related to gel leakage during gel retrieval were recorded. The final gel weight was then divided by the initial gel weight to calculate gel retrieval percentage. Each implant was weighed three times.

b. retrieval from phantom tissue

A 1.5 ml Eppendorf was weighed on a OHAUS® GA200D scale, set to 4 significant digits, and the resulting weight was then tared. A visual reference for 75 µl was created by dispensing 75 µl of water in a 1.5 ml Eppendorf. Gel was then dispensed in the previously tared Eppendorf until it matched the water filled Eppendorf as closely as possible. The gel-filled Eppendorf was then placed on the scale and the weight recorded. The trocar was used to make an insertion into the phantom tissue and form a tunnel-shaped space. The metal, sharp part of the trocar was removed, leaving only the cannula inserted firmly in place. The gel was then injected into the implant, which was subsequently placed on the cannula and pushed into the phantom tissue by the stem. Any observations of gel leakage during injection were recorded. While the implant was incubated in the phantom tissue for 3 minutes, the residual gel in the Eppendorf was weighed and calculated. Afterwards, the gel was retrieved from the implant while it remained in the phantom tissue and placed into the Eppendorf. Any observations of gel leakage during retrieval were recorded. The Eppendorf was then weighed and the final gel weight was recorded. The residual gel was subtracted from the initial and final weights. The gel retrieval

percentage was calculated by dividing the final gel weight by the initial gel weight. Each implant was weighed three times.

c. retrieval from murine subcutaneous space

A 1.5 ml Eppendorf was weighed on an OHAUS® GA200D scale, set to 4 significant digits, and the resulting weight was then tared. A visual reference for 100 µl was created by dispensing 100 µl of water in a 1.5 ml Eppendorf. Gel was then dispensed in the previously tared Eppendorf until it matched the water filled Eppendorf as closely as possible. The gel-filled Eppendorf was then placed on the scale and the weight recorded. A surgical knife was used to make a small incision, approximately 5 mm, to allow insertion of the trocar device. After the incision, the trocar device was used to make a tunnel shaped space. The metal part was then removed, leaving the cannula in place in the subcutaneous tissue. The gel from the Eppendorf was then injected into the implant. The implant was placed in the cannula and pushed down with a stem. While the implant was in the subcutaneous tissue, the residual gel was weighed on the scale and its weight recorded. Then, the gel was retrieved from the implant, while the implant was in the subcutaneous tissue, and placed in the Eppendorf with residual gel. Its weight was then recorded. The residual weight was removed from both the initial and final weight, then the retrieval percentage was calculated. This was repeated three times for both the control and experimental group. Alternatively, instead of retrieving the gel from the implant while it was inside, the implant was removed from the subcutaneous space and then the gel was retrieved. The gel was then weighed to calculate the final weight, which was then divided

by the initial weight to calculate the retrieval percentage. This was also repeated three times for both the experimental and control groups.

4.2.3 Statistics

All statistical calculations were done on Microsoft Excel 2017. A two-way ANOVA with replication was done for the assessment of all experimental groups, which included all cage-like and capsule groups, and location of gel retrieval (inside or outside phantom) on percentage of gel retrieval. The ANOVA was then followed by comparisons with t-tests to assess which comparisons showed significance. Significance values were given at $p<0.05$ * and $p<0.01$*

4.3 Results

4.3.1 Retrieval from implant alone

The results for retrieval from the implant alone is shown in Figure 4.1. Capsule-3 had higher gel retrieval than Cage-1 ($p<0.05$) and Cage-2 ($p<0.05$), Capsule-1 had higher gel retrieval than Cage-1 ($p<0.05$) and Cage-2 ($p<0.05$), and Capsule-2 had higher gel retrieval than Cage-1 ($p<0.01$) and Cage-2 ($p<0.01$).

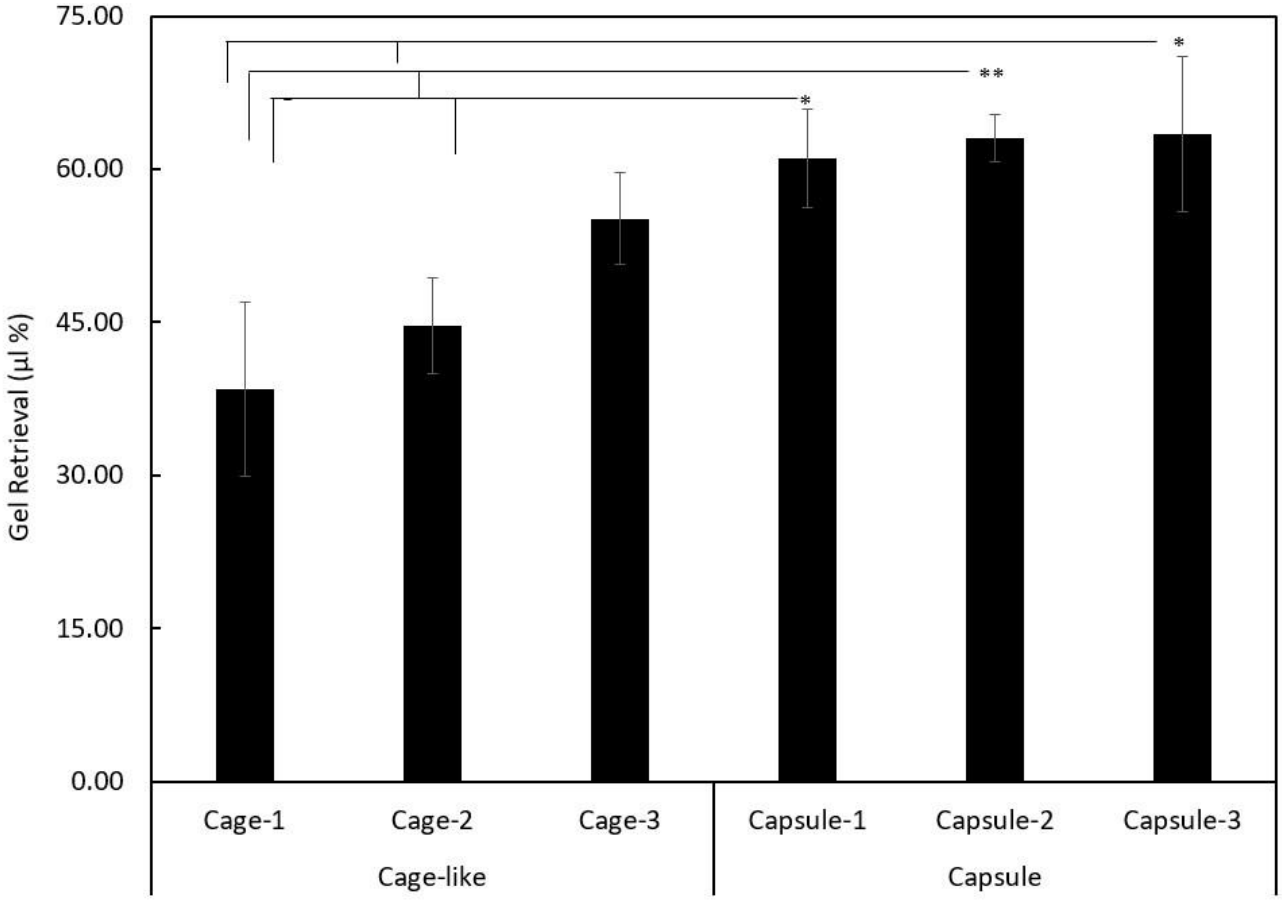

Figure 4.1 Retrieval of gel from implant alone. Retrieval percentage (µl%) is amount of gel retrieved from an injected amount of 75 µl. Significant values are set at $p<0.05$ *, $p<0.01$ **

4.3.2 Retrieval from phantom tissue

Figure 4.2 shows the trocar device and phantom tissue used for this study. The same trocar device was also used in the murine subcutaneous space study.

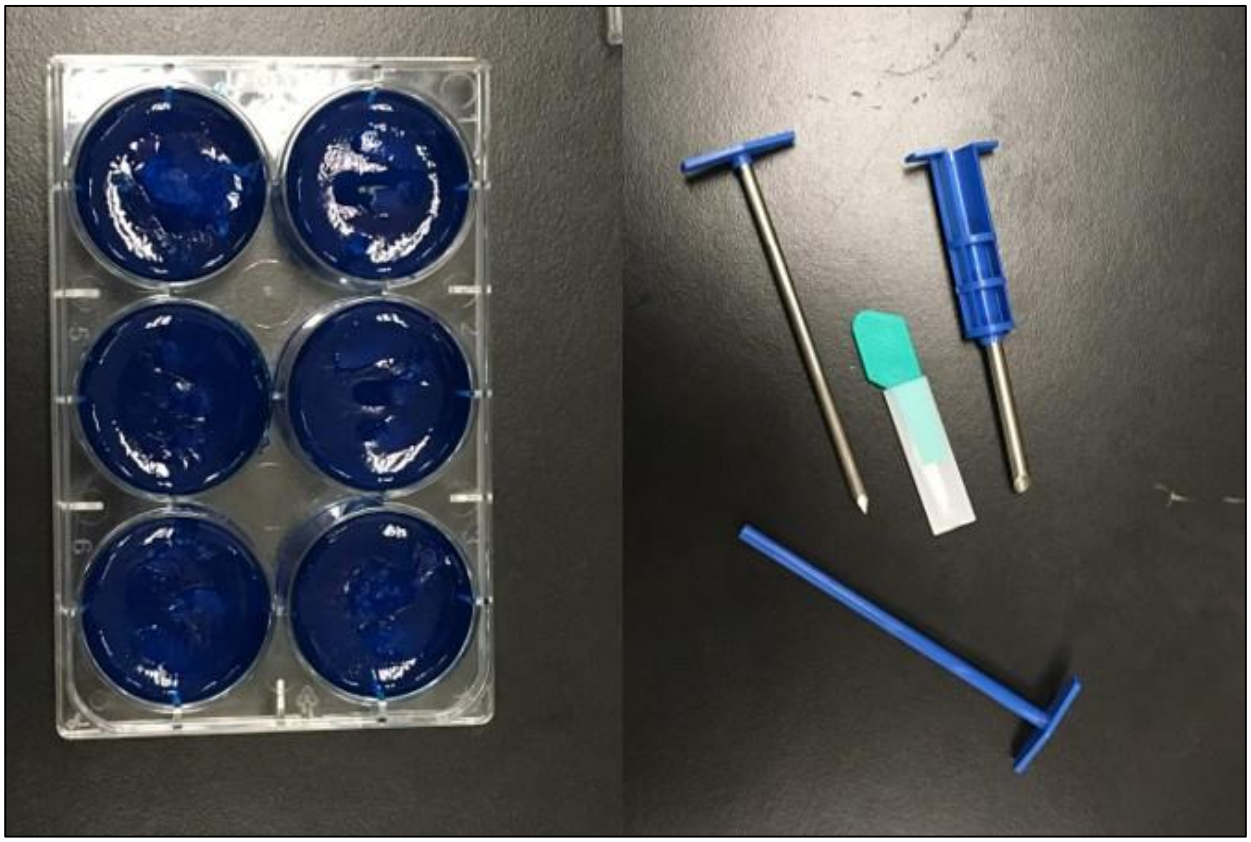

Figure 4.2 Materials pertinent to the study include (left) 8% Gelatin-1% Agar-0.24% formaldehyde and a (right) trocar based device consisting of a stem, cannula, and metal trocar piece. The surgical knife in the middle of the device was used for making incisions in the murine specimen.

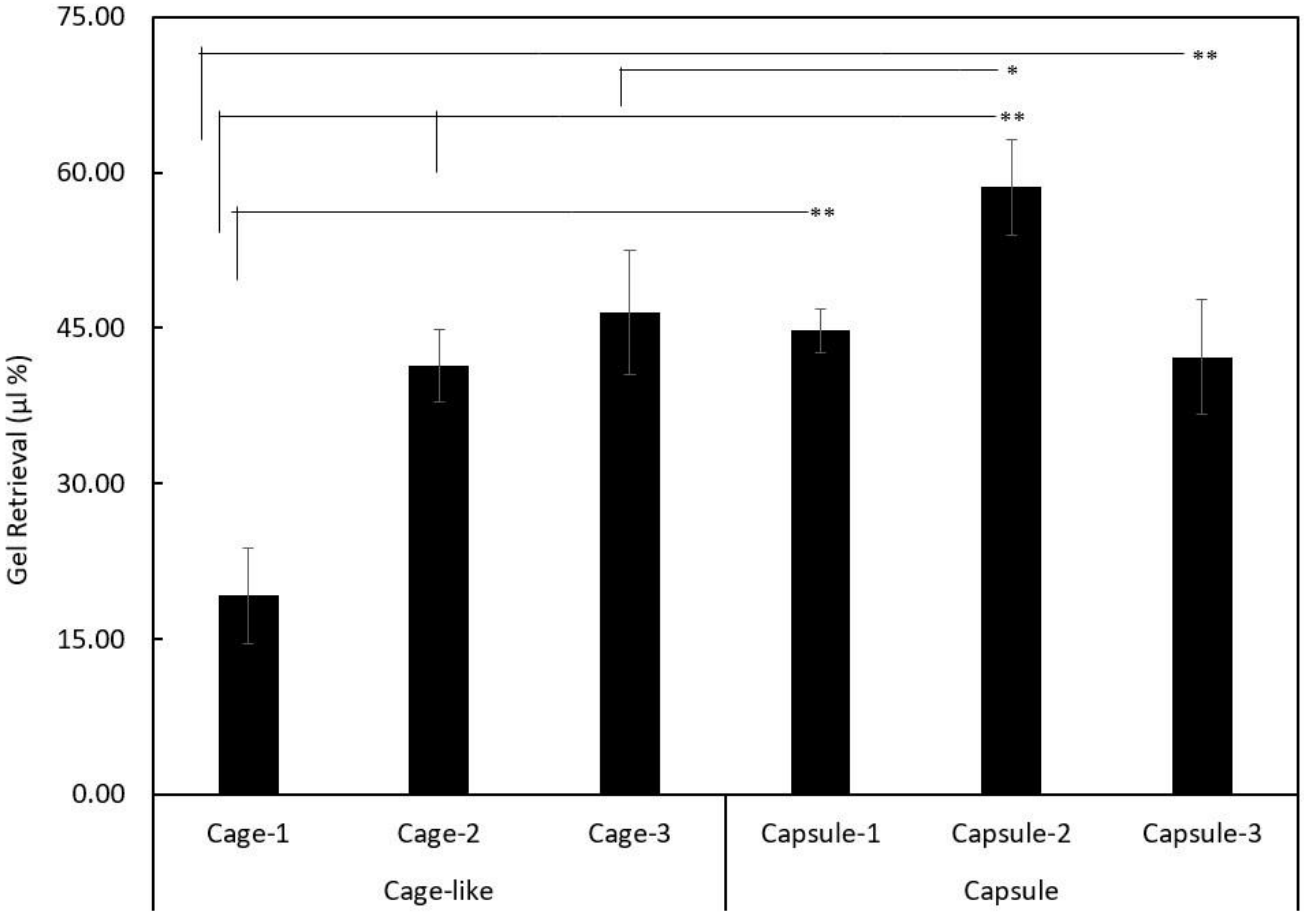

Figure 4.3 Retrieval of gel from phantom tissue. Retrieval percentage (µl%) refers to the amount of gel retrieved from an injected amount of 75 µl. Significant values are set at $p<0.05$ *, $p<0.01$ **

Gel retrieval from phantom tissue is shown in Figure 4.3. All capsule designs had more gel retrieval than Cage-1 ($p<0.01$). However, only Capsule-2 had more gel retrieval than Cage-2 ($p<0.01$) and Cage-3 ($p<0.05$).

4.3.3 Retrieval within design group

Gel retrieval within cage-like implants is shown in Figure 4.4. Cage-3 had more gel retrieval from implant alone than Cage-2 ($p<0.05$) and Cage-1 ($p<0.05$) as well as more gel retrieval from phantom than Cage-1 ($p<0.01$). Cage-2 had more gel retrieval from phantom than Cage-1 ($p<0.01$). Cage-1 had less gel retrieval from phantom and implant alone compared to the other groups and also had more gel retrieval from implant alone versus phantom ($p<0.05$). Cage-3 and Cage-2 had consistent gel retrieval when comparing from implant alone versus phantom.

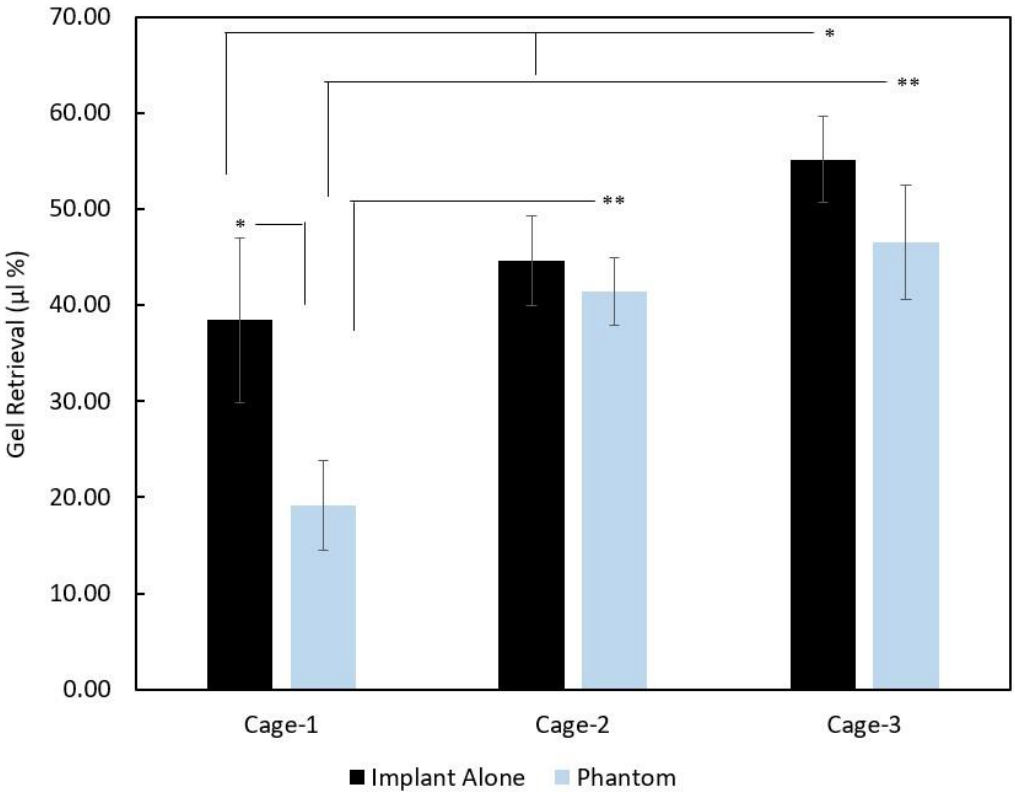

Figure 4.4 Retrieval of gel in cage-like from implant alone or phantom tissue. Retrieval percentage (µl%) refers to the amount of gel retrieved from an injected amount of 75 µl. Significant values are set at $p<0.05$ *, $p<0.01$ *

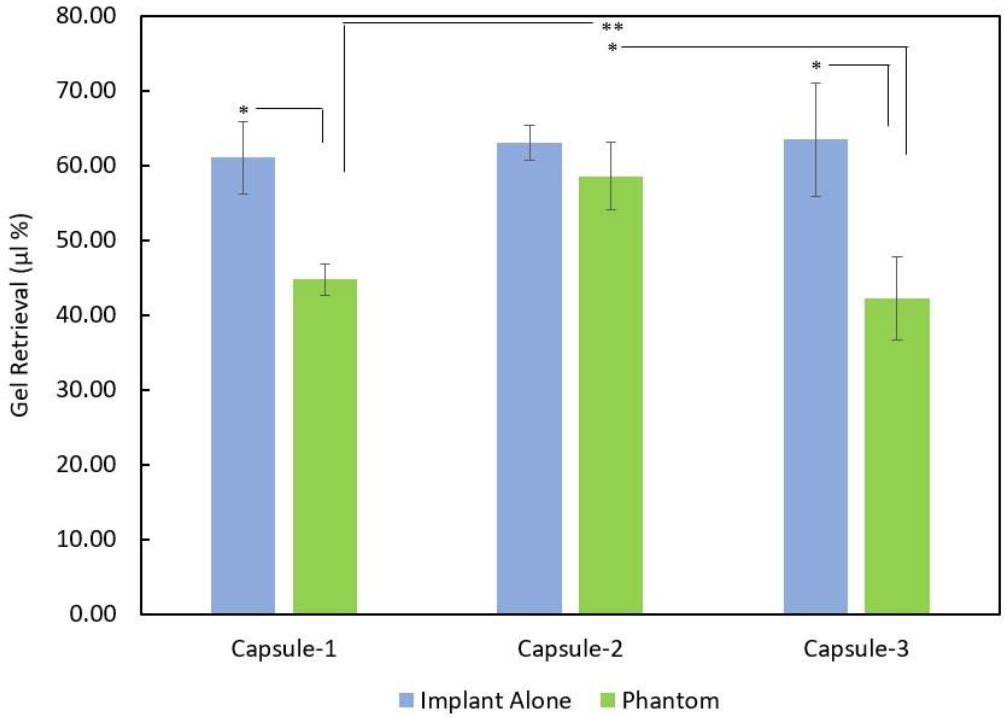

Figure 4.5 Retrieval of gel in capsule from implant alone or phantom. Retrieval percentage (µl%) refers to the amount of gel retrieved from an injected amount of 75 µl. Significant values are set at $p<0.05$ *, $p<0.01$ **

When assessing within the capsule group (Figure 4.5), Capsule-2 had more gel retrieval from phantom than Capsule-1 ($p<0.01$) and Capsule-3 ($p<0.05$). Additionally, there was no significant difference in gel retrieval for Capsule-2 when comparing from implant alone versus phantom tissue. However, both Capsule-3 and Capsule-1 had a significant difference between retrieval from implant alone and phantom tissue ($p<0.05$).

4.3.4 Retrieval from murine subcutaneous tissue

The final prototype, which was based on Capsule-2, and the control are shown in Figure 4.6.

Figure 4.6 The final prototype CAD design (top-left), final prototype print (bottom-left), control CAD design (top-right), and control print (bottom-right).

The characteristics of the final prototype and control are summarized in Table 4.2

Table 4.2 Summary of final prototype and control characteristics

Implant Type	Final Prototype	Control
CAD Pore Area	2.54mm^2	0mm^2
Actual Pore Area	2.22mm^2	0mm^2
CAD Total Pore Area/Surface Area	45%	7.00%
Actual Total Pore Area/Surface Area	40%	7.00%
CAD # of Open Pores	28	1
Actual # of Open Pores	28	1
% Loss Open Pores	0%	0%
% Loss Pore Area	13%	0%
% Loss Total Pore Area/Surface Area	11%	0%
Shape of Pore	circular	none
Smoothing	no	no

The gel retrieval was much higher in non-porous control (~7% total pore area/surface area due to injection opening) than experimental from subcutaneous space ($p<0.01$) and implant alone ($p<0.01$), as seen in Figure 4.7.

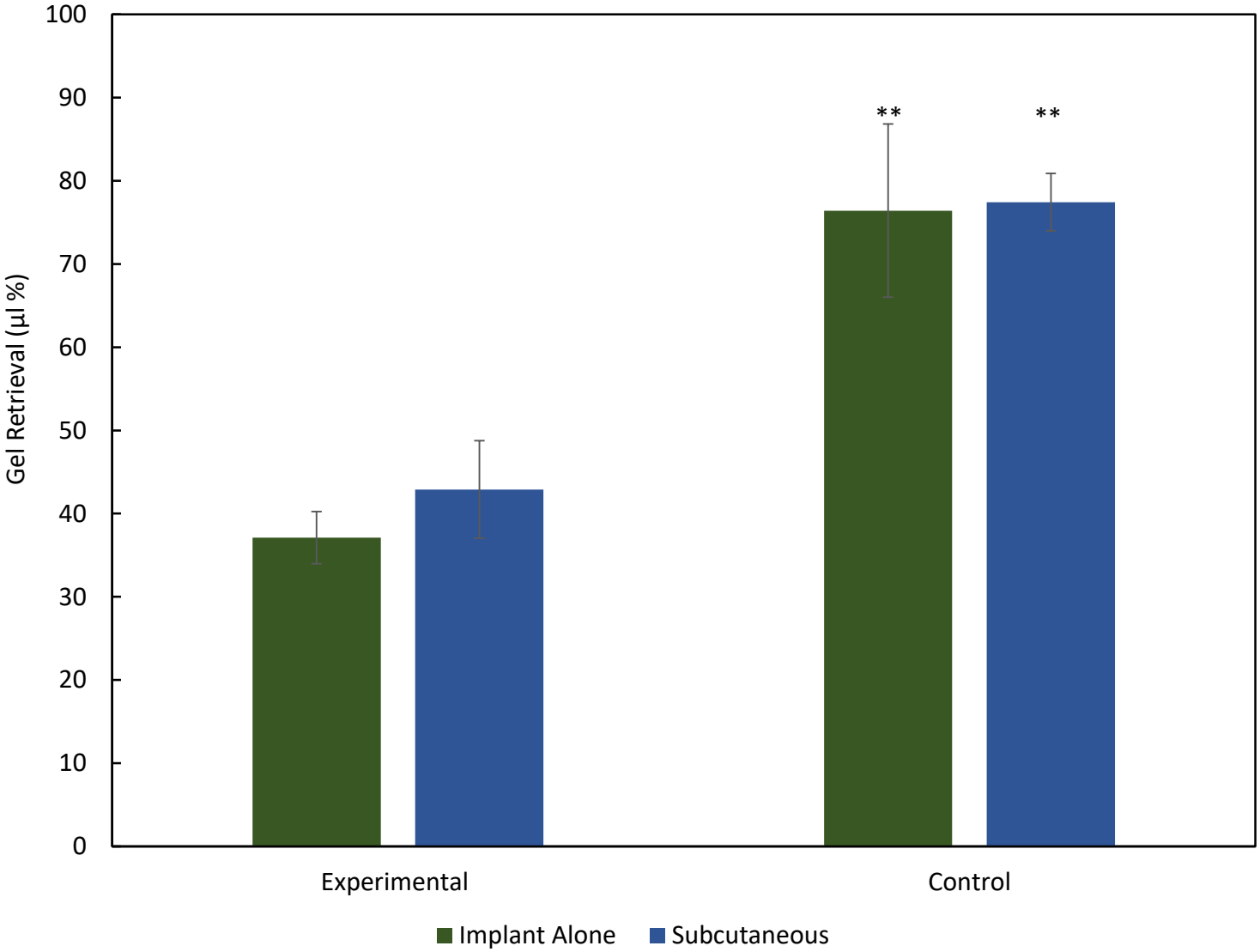

Figure 4.7 Gel retrieval from implant alone and murine subcutaneous space. Gel was retrieved from implant while inside the subcutaneous space or after it was inserted and removed from subcutaneous space (implant alone). Retrieval percentage (µl%) refers to the amount of gel retrieved from an injected amount of 100 µl. Significant values are set at $p<0.05$ *, $p<0.01$ **

4.4 Discussion

4.4.1 Retrieval from implant alone capsule vs cage-like

The capsule design was the best in gel retrieval from the implant alone when compared to cage-like. One reason that explains the results could be that the implants were set on a paper towel after the injection of the gel. This was done to account for gel leakage that could happen when the implant was incubated for 3 minutes. It was also noted that the paper towel could be absorbing the gel and since the cage-like had long axial openings, it was more prone to gel loss due to contact with surfaces. This would explain why Cage-3, which had the smallest gap area, had similar gel retrieval when compared to the capsule designs. However, that is not to say that gel could not be lost from the capsule designs as well, as gel did leak from them as well. One main factor that would affect the gel retrieval runs was the injection technique. If the gel was placed too fast and in one corner of either implant design, it would leak very easily during injection or after its incubation on the paper towel. A big difference between both designs was the fact that it was easier to make mistakes with the cage-like. Accordingly, more trials were usually required with the cage-like designs and the runs were repeated until a consistent retrieval percentage was attained. The capsule design did have one main flaw, and that was the pores placed on the end converse to the injection port. When the gel was injected too fast or non-uniformly, the gel would mainly leak through there in all designs. However, the capsular design also made it easier for surface tension to keep the gel inside, since the pores were smaller and would allow less gel flow towards the surface of the pores. It also must be noted that gel would stick to the insides of all implants regardless of technique or other

characteristics. This was one advantage that the cage-like had over the capsule design, since it was much easier to absorb gel that is stuck on the inside of the implant. Even so, the capsule design was overall still better than the cage-like in gel retrieval.

4.4.2 Retrieval from phantom capsule vs cage-like

Retrieval was once again better in the capsule design versus the cage-like design. One main factor that affected the gel retrieval was delivery via the trocar. Since all implants had to contact and slide along the cannula, it is not surprising that the cage-like would lose much of the gel during the delivery. The cage-like had too much open pore space due to its gaps, so it was very easy to retrieve the gel from different angles and there was also less surface tension on the gel, making it easier to retrieve more gel. However, the open space also was more prone to gel loss and less retention of it once inside the phantom. Also, Capsule-2 was the only design that was greater than all cage-like designs in terms of gel retrieval, whereas the other two capsule designs were only significantly better than Cage-1 ($p<0.01$), the least efficient cage-like design. Capsule-2 was the median group in terms of pore diameter, and this particular diameter seemed to be relatively effective for retaining the gel and also allowing retrieval since the pores are not too small, which would lead to higher surface tension in the pores.

4.4.3 Retrieval within design group

Retrieval from the cage-like was most efficient in Cage-3. It was the most stable of the three, and the gaps were not too wide, which would lead to less gel contact with surfaces. The

fact that gel retrieval was higher from implant alone would be due to the easier accessibility to the gel through the long gaps, which was true for all designs. However, Cage-3 did have higher retention due to its smaller gaps, so the complementary effect of long accessible gaps and a stable hold on the gel led to a higher retrieval percentage from implant alone when compared to the two other groups. The converse would be true when comparing gel retrieval from phantom among the capsule designs. That is, the main factor limiting retrieval from the phantom for the capsule designs was accessibility and possibly pore surface tension retaining too much of the gel. All implants could only have the gel retrieved from one end of the implant while inside the phantom tissue, which was very different outside, where they were all comparable. The reason the capsule designs were very comparable from the implant alone is because there is more accessibility and gel can get retrieved from the pores, whereas in the phantom tissue, there are less angles from which gel can be retrieved, especially gel stuck inside the pores. It is likely that the Capsule-3 pores were too big and allowed too much contact with the trocar device cannula, hence its significant difference ($p<0.05$) in retrieval from phantom and implant alone. Additionally, although Capsule-1 has smaller pores and should have less bound on the surface, it had significantly ($p<0.01$) lower gel retrieval than Capsule-2 from phantom tissue and a significant difference (0.05) between retrieval from phantom and implant alone. The reasoning is that the Capsule-2 pores have less surface tension in them. Namely, the retrieval pulls out all the gel from the pores of the implant since it can interact more efficiently with the gel in the core of the implant. Capsule-1 on the other hand, has more pores and higher pore surface tension. Although its pores should retain less gel, they are more

numerous. The end result is more gel that is tightly retained inside the pores versus the retained gel in Capsule-2 pores. Capsule-2 also was the only capsule implant that did not have a significant difference between retrieval from phantom and implant alone, meaning that it is more consistent.

4.4.4 Retrieval from murine subcutaneous tissue

Capsule-2 was the most efficient implant, so its design was the basis for the final prototype. Despite the promising results in phantom tissue and from the implant alone. The final prototype still needs further optimization. As was seen in its comparison with the control group, the gel retrieval was much less from implant alone ($p<0.01$) and subcutaneous space ($p<0.01$). Clearly, more modifications must be made so that the experimental group is similar to the control. A particular modification that could reduce the exposure of gel on the surface could be the use of drafted holes. This could allow increased surface tension that will keep the gel inside the implant and reduce gel entering and getting stuck in the pores. Another possible modification could be the thickness since a higher thickness will lead to a longer barrier between the subcutaneous tissue and the inner space of the implant. A combination of a drafted hole with a larger thickness would be an interesting approach to attempt. Also, the viscosity of the hydrogel or solution to be placed inside the body could affect the way that it is retained in the implant, as seen in the control group runs, which led to about 25% gel loss.

Chapter 5

Conclusion

The objective of the study was to produce a PLA based implant for effectively injecting, allowing retrieval, and enabling retention of the gel inside of the subcutaneous space. Many designs were considered for different reasons, such as the capsule slotted design for increasing total pore area/surface area the most possible, the cage-like for increased accessibility, and the circular capsule design to minimize gel exposure on pore surface. Although the study elucidated the effect of pore and gap area on the ability to retain gel and retrieve it, as well as that printing implants with a diameter of 1.2 mm or higher is reproducible in terms of open pore number, total pore area/surface area, and pore area, more work is needed to optimize the implant for delivering a hydrogel for cancer cell detection. Different tactics for increasing gel retrieval are drafted holes, increased thickness, and a smaller nozzle diameter. Different fabrications methods can also be used to create smaller pores that were not possible with FDM. It must also be noted that all injections were done with a micropipette p200, which is not conventional in the clinical setting. For the purposes of studying the effect of the implant design it is understandable to use a micropipette, but if this implant and its complementary gel are to be marketed it is imperative that a sterile clinical instrument, such as a 18G syringe needle, be used efficiently. Indeed, this is another milestone that needs to be reached to further develop this implantable device. Other future directions involve studying retention of gels with different viscosities, cell migration studies to assess entry of cells into the implant, and ultimately *in vivo* studies with injected metastatic cancer cells.

References

Adamczak, S.; Zmarzly, P.; Stepien, K. (2016). “Identification and analysis of optimal method parameters of the V-block waviness measurements.” Bulletin of the Polish Academy of Sciences Technical Science **64** (2): 45-52

Azarin, S. M.; Yi, J.; Gower, R. M.; Aguado, B. A.; Sullivan, M. E.; Goodman, A. G.; Jiang, E. J.; Rao, S. S.; Ren, Y.; Tucker, S. L.; Backman, V.; Jeruss, J. S.; Shea,L.D.(2015)."In vivo capture and label-free detection of early metastatic cells." Nature Communications **6**: 8094-8113.

Azimi, P.; Zhao, D.; Pouzet, C.; Crain, N.E.; Stephens,B. (2016). "Emissions of ultrafine particles and volatile organic compounds from commercially available desktop three-dimensional printers with multiple filaments." Environ Sci Technol **50**(3): 1260-1268.

Buck, C. B. and D. R. Lowy (2011). "Immune readouts may have prognostic value for the course of merkel cell carcinoma, a virally associated disease." J Clin Oncol **29**(12): 1506-1508.

Chen, A. I.; Balter, M.L.; Chen, M.I.; Gross, D.; Alam, S. K.; Maguire, T. J.; Yarmush, M. L. (2016). "Multilayered tissue mimicking skin and vessel phantoms with tunable mechanical, optical, and acoustic properties." Med Phys **43**(6): 3117-3131.

Chen, W.; Weng, S.; Zhang, F.; Allen, S.; Li, X.; Bao, L.; Lam, R.H.W.; Macoska, J.A.; Merajver, S.D.; Fu, J. (2013). "Nanoroughened surfaces for efficient capture of circulating tumor cells without using capture antibodies." ACS Nano **7**(1): 566-575.

Christiyan, K.J.; Chandrasekhar, U.; Venkateswarlu, K. (2016). “A study on the influence of process parameters on the mechanical properties of 3D printed ABS composite.” IOP Conf. Series: Materials Science and Engineering **114**:12-19

Dong, G.; Wijaya, G.; Tang, Y.; Zhao, Y. F. (2018). "Optimizing process parameters of fused deposition modeling by Taguchi method for the fabrication of lattice structures." Additive Manufacturing **19**: 62-72.

Fass, L. (2008). “Imaging and cancer: a review.” Mol Oncol **2**(2): 115-152

Gremare, A. G., V.; Bareille, R; Heroguez, V.; Latour, S.; L'heureux, N.; Fricain, J. C.; Catros, S.; Le Nihouannen, D. (2018). “Characterization of printed PLA scaffolds for bone tissue engineering.” J Biomed Mater Res A. **106:** 887-894.

Holland, G.;Meyer, F. (1932). “Der gewebsdruck beim odem”. Arch. f. exper. Path. u. Pharmakol., **168:**603.

Hong, B.; Zu, Y. (2013). “Detecting circulating tumor cells: current challenges and new trends”. Theranostics **3**(6):377-394.

Jasiuk, I.; Abueidda, D. W.; Kozuch, C.; Pang, S.; Su, F. Y.; McKittrick, J.(2018). "An overview on additive manufacturing of polymers." Jom **70**(3): 275-283.

Kim, Y.; Yoon, C.; Ham, S.; Park, J.; Kim, S.; Kwon, O.; Tsai, PJ. (2015). "Emissions of nanoparticles and gaseous material from 3D printer operation." Environ Sci Technol **49**(20): 12044-12053.

Kleiner, L. W.; Wright, J. C.; Wang, Y. (2014). “Evolution of implantable and insertable drug delivery systems.” Journal of Controlled Release **181**:1-10

Ko, C. Y.; Wu, L.; Nair, A. M.; Tsai, Y.; Lin, V. K.; Tang, L. (2012). "The use of chemokine-releasing tissue engineering scaffolds in a model of inflammatory response-mediated melanoma cancer metastasis." Biomaterials **33**(3): 876-885

Kozior, T.; Kundera, C. (2017). “Evaluation of the influence of parameters of FDM technology on the selected mechanical properties of models.” Procedia Engineering **192**: 463-468

Kumar, V.; Abbas A. K.; Fausto, N.; Robbins, S. L.; Cotran, R. S. (2005). “Robbins and Cotran pathologic basis of disease (7th ed.)” Philadelphia: Elsevier Saunders.

Kundera, Cz.; Bochnia, J. (2014). “Investigating the stress relaxation of photopolymer O-ring seal models.” Rapid Prototyping Journal **20** (6): 533-540

Kundera, Cz.; Kozior, T. (2014). “Research of the elastic properties of bellows made in SLS technology.” Advanced Materials Research **874**: 77-81

Kuznetsov, V.; Solonin, A. N.; Urzhumtsev, O. D.; Schilling, R.; Tavitov, A. G. (2018). "Strength of PLA components fabricated with fused deposition technology using a desktop 3D printer as a function of geometrical parameters of the process." Polymers **10**(3): 313.

Leong, K. F. C., C. K.; Sudarmadji, N.; Yeong, W. Y. (2008). "Engineering functionally graded tissue engineering scaffolds." Journal of the Mechanical Behavior of Biomedical Materials **1**(2): 140-152.

MakerBot. *PLA and ABS Strength Data*. http://download.makerbot.com/legal/MakerBot_R__PLA_and_ABS_Strength_Data

Meyer, F., and Holland, G. (1932). “Die Messung des Druckes in Geweben. Arch.” f. exper. Path. u.Pharmakol., **168:** 580.

Norman, J.; Madurawe, R.D.; Moore, C.M.; Khan, M.A.; Khairuzzaman, A. (2017). "A new chapter in pharmaceutical manufacturing: 3D-printed drug products." Adv Drug Deliv Rev **108**:39-50.

Olszewski, W.L..; Ambujam, G.; Jain, P.; Zaleska, M.; Cakala, M.; Gradalski, T. (2010). "Tissue fluid pressure and flow in the subcutaneous tisue in lymphedema-hints for manual and pneumatic compression therapy." Phlebolymphology **17**(3): 7.

Pilipchuk, S.P.; Vaicik, M.K.; Larson, J.C.; Gazyakan, E.; Cheng, MH.; Brey, E.M. (2013). “Influence of crosslinking on the stiffness and degradation of dermis derived hydrogels.” Journal of Biomedical Materials Research **101**(10): 2883-2889

Steinle, P. (2016). "Characterization of emissions from a desktop 3D printer and indoor air measurements in office settings." J Occup Environ Hyg **13**(2): 121-132.

Rao, S. S.; Bushnell, G.G.; Azarin, S.M.; Spicer, G.; Aguado, B.A.; Stoehr, J.R.; Jiang, E.J.; Backman, V.; Shea, L.D.; Jeruss, J.S. (2016). "Enhanced survival with implantable scaffolds that capture metastatic breast cancer Cells in vivo." Cancer Res **76**(18): 5209-5218.

Tang, L. (2015). *US Patent No 20150283073*. Arlington, TX: U.S. Patent and Trademark Office

Tymrak, B.M.; Kreiger, M.; Pearce, J.M. (2014). "Mechanical properties of components fabricated with open-source 3-D printers under realistic environmental conditions." Materials & Design **58**: 242-246.

Wells, H. S.; Youmans, J. B.; Miller, D. G. (1938). “Tissue Pressure (intracutaneous, subcutaneous, and intramuscular) as related to venous pressure, capillary filtration, and other factors”. Journal of Clinical Investigation, 17(4):489–499.

Wicha M. S.; Hayes D. F. (2011). “Circulating tumor cells: not all detected cells are bad and not all bad cells are detected.” J Clin Oncol 29(12):1508-1511.

Yang, S.; Leong, K. F.; Du, Z.; Chua, C. K. (2001). "The design of scaffolds for use in tissue engineering. part I. traditional factors." Tissue Engineering **7**(6): 679-689.

Yang, S.; Leong, K. F.; Du, Z.; Chua, C. K. (2002). "The design of scaffolds for use in tissue engineering. part II rapid prototyping techniques." Tissue Engineering **8**(1).

Yeong, W. Y.; Chua, CK.; Leong, KF.; Chandrasekaran, M. (2004). "Rapid prototyping in tissue engineering: challenges and potential." Trends Biotechnol **22**(12): 643-652.